Stochastic Geometry-based Uplink Analysis of Massive MIMO Systems with Fractional Pilot Reuse

Priyabrata Parida and Harpreet S. Dhillon.

***Abstract*—In this work, we analyze the performance of the uplink (UL) of a massive MIMO network considering an asymptotically large number of antennas at base stations (BSs). We model the locations of BSs as a homogeneous Poisson point process (PPP) and assume that their service regions are limited to their respective Poisson-Voronoi cells (PVCs). Further, for each PVC, based on a threshold radius, we model the *cell center* (CC) region as the *Johnson-Mehl* (JM) cell of its BS while rest of the PVC is deemed as the *cell edge* (CE) region. The CC and CE users are located uniformly at random independently of each other in the JM cell and CE region, respectively. In addition, we consider a fractional pilot reuse (FPR) scheme where two different sets of pilot sequences are used for CC and CE users with the objective of reducing the interference due to pilot contamination for CE users. Based on the above system model, we derive analytical expressions for the UL signal-to-interference-and-noise ratio (SINR) coverage probability and average spectral efficiency (SE) for randomly selected CC and CE users. In addition, we present an approximate expression for the average cell SE. One of the key intermediate results in our analysis is the approximate but accurate characterization of the distributions of the CC and CE areas of a typical cell. Another key intermediate step is the accurate characterization of the pair correlation functions of the point processes formed by the interfering CC and CE users that subsequently enables the coverage probability analysis. From our system analysis, we present a partitioning rule for the number of pilot sequences to be used for CC and CE users as a function of threshold radius that improves the average CE user SE while achieving similar CC user SE with respect to unity pilot reuse.**

***Index Terms*—Stochastic geometry, Massive MIMO, uplink, fractional pilot reuse, cellular network, coverage probability, cell spectral efficiency, Poisson point process, pair correlation function.**

I. Introduction

Owing to its ability to improve both spectral and energy efficiency of wireless networks, massive multiple-input multiple-output (mMIMO) is considered a key enabler of the fifth-generation (5G) communication systems and beyond. Fundamentally, mMIMO is a multi-user MIMO system where a large number of antennas at the base stations (BSs) are used to simultaneously serve a fewer number of users (compared to the number of antennas at the BSs). Although a simple extension of conventional multi-user MIMO technique, it is set to revolutionalize wireless communication networks as it has been proven that under ideal conditions it eliminates the deleterious effect of channel fading and additive noise while negating the effect of network interference [2]–[4]. In order to decode the simultaneously transmitted data from different users, each BS requires the channel knowledge of the users attached to it that is estimated through a set of orthogonal pilot sequences. Due to limited channel coherence interval, the number of orthogonal pilot sequences is also limited. As a result, the pilot sequences need to be reused across different cells. In his seminal work [2], Marzetta showed that under the assumption of independent and identically distributed (i.i.d.) Rayleigh fading across BS antennas and sub-optimal low-complexity processing schemes such as maximal ratio combining (MRC), the reuse of pilot sequences gives rise to an inherent interference known as *pilot contamination* (PC), which fundamentally limits the performance of mMIMO networks. As discussed next in detail, a significant amount of research effort has been focused on overcoming the effect of PC. Amongst all the solutions, a relatively simple scheme, namely fractional pilot reuse (FPR), stands out in reducing the effect of PC for the cell edge (CE) users. Hence, the objective of this article is to analyze the performance of a mMIMO network that uses the FPR scheme.

A. Motivation and related works

In the literature, PC suppression or mitigation methods can be broadly categorized into protocol based methods [5], BS coordination based methods [6], [7], and pilot reuse or hopping based methods [8], [9]. Please refer to [10] for a comprehensive survey on this subject. While protocol and coordination based methods are effective in removing the PC, they are usually complex. Further, these techniques require some degree of coordination among BSs. On the other hand, the gains obtained by pilot hopping based methods is primarily due to interference randomization and is hence limited to scenarios with larger channel coherence times. In contrast, a low complexity and distributed scheme to counter the effect of PC is to forbid reusing the same pilots in every cell, which requires no coordination among BSs [11], [12]. The concept of pilot reuse is similar to the frequency reuse in cellular networks. In [11], the optimal pilot reuse factor is obtained for a network with linear topology. From the numerical simulations, authors show that higher than unity pilot reuse factor is beneficial for average cell throughput. In [12], for a hexagonal cellular network model, authors show that reuse-1 may not be optimal in all scenarios. These works considered the use of completely orthogonal sets of pilots in neighboring cells. However, the spectral efficiency (SE) can be further improved by using a more aggressive pilot reuse scheme, namely FPR, instead of

The authors are with Wireless@VT, Department of ECE, Virginia Tech, Blacksburg, VA. Email: {pparida, hdhillon}@vt.edu. The support of the US NSF (Grant ECCS-1731711) is gratefully acknowledged. This paper is presented in part at the IEEE International Conference in Communications (ICC), 2018 [1].

completely orthogonal reuse across cells. Conceptually, FPR is similar to that of fractional frequency reuse (FFR) used in LTE systems to mitigate the effect of inter-cell interference. To the best of the knowledge of the authors, the concept of FPR was first introduced in [13]. In FPR, similar to FFR, depending on the channel condition, users in a cell are classified into two categories, namely cell center (CC) and CE users. While the set of pilots reserved for CC users are reused in every cell, the set of pilots for CE users are reused in specific cells depending upon the reuse factor.

For the performance analysis of mMIMO systems with FPR, it is imperative to consider a large-scale multi-cell setup so that the effect of interference on the performance can be accurately modeled. For such problems, stochastic geometry provides a rigorous set of tools for the spatial modeling and performance analysis, as discussed in detail in [14], [15]. For a pedagogical treatment of the subject with emphasis on the application to cellular network, interested readers are advised to refer to [14]. Although stochastic geometry has been used for the performance analysis of mMIMO systems in [16]–[25], the analyses presented in these works cannot be trivially extended to analyze the FPR scheme. To begin with, in contrast to our network topology, in [25] a cooperative mMIMO network is considered. In [16]–[22], where a cellular topology is considered, the UL interference field generated by the users from unity pilot reuse scheme is different from the FPR scheme. Further, the analyses [17]–[22] are limited to the consideration of a fixed number of users in each BS which does not take into account the varying load (number of users) in each cell. In this work, we propose a new approach to analyze the performance of a cellular mMIMO network considering FPR scheme that results in the following key contributions.

B. Contributions of the work

1) Analytical model for UL analysis of a mMIMO system with FPR: A new generative model is proposed to analyze the performance of the UL of a mMIMO system in the asymptotic antenna regime under the consideration of FPR scheme. We model the BS locations as a Poisson point process (PPP). Based on a threshold distance R_c, we characterize the CC regions as the Johnson-Mehl (JM) cells associated with the BSs. The complementary region in each cell is modeled as the CE region. One important result in our analyses is the approximate but accurate distribution functions for the CC and CE areas of a typical Poisson-Voronoi Cell (PVC). These results are subsequently used to model the load (number of CC and CE users) distribution of each cell. Using these distributions, we provide key intermediate results, such as the pilot assignment probability to a randomly selected CC (CE) user and utilization probability of a pilot. These results are later used in the coverage probability and SE analyses.

*2) Signal-to-interference-plus-noise ratio (*SINR*) coverage, average user and cell SEs analysis:* We present SINR coverage probability of a user assigned to a given CC (CE) pilot. The derivation of exact probability is difficult as the exact statistical characterization of the interference field is extremely challenging. In fact, derivation of this result for a relatively simpler scenario of the classical UL system, where the segregation between CC and CE users is not present, is also intractable. Hence, to lend tractability to this problem, we resort to a careful approximation of the interference statistics in the UL. Motivated by [26], first, we derive the pair correlation function (PCF) of the interfering user locations with respect to (w.r.t.) the BS of interest. Using this PCF, we approximate the point process formed by the CC (CE) interfering users as a non-homogeneous PPP. Next, based on the *dominant interferer* based approach, we provide useful theoretical expressions for the coverage probability of a user assigned to a CC (CE) pilot. This result is extended to obtain analytical expressions for the average SEs of a randomly selected CC (CE) user and average SE of a typical cell.

3) System design guidelines: Our analysis leads to following system design guidelines. First, our analyses show that for a certain range of threshold radius by allocating $1-\exp(-c_2\pi\lambda_0 R_c^2)$, where λ_0 is the BS density and c_2 is a constant, fraction of pilots for the CC users, FPR scheme improves the average SE of a CE user with marginal reduction in the average SE of a CC user compared to unity reuse. Second, for a given threshold radius, it is possible to achieve higher average cell SE using FPR scheme compared to unity reuse by a suitable partitioning (different from the aforementioned rule) of the set of the pilots. Third, the coverage probability of a user on a CE pilot decreases with increasing R_c in the higher SINR regime, however, the reverse trend is observed for the lower SINR regime.

II. System Model

A. Network model

1) BS and user locations: In this work, we analyze the UL performance of a cellular network where each BS is equipped with $M \to \infty$ antennas. The locations of the BSs belong to the set $\Psi_b = \Phi_b \cup \{\mathbf{o}\}$, where $\mathbf{o}$ represents the origin, and Φ_b is a realization of homogeneous PPP of density λ_0. In this work, we present our analysis condition on the location of the BS at $\mathbf{o}$. By virtue of Slivnyak's theorem, the reduced palm measure of Ψ_b is equal to the original measure of Φ_b [27]. The location of the j-th BS is denoted by $\mathbf{b}_j \in \Psi_b$, where the index j does not represent any ordering and $\mathbf{b}_0 = \mathbf{o}$. In a cell, the region that is within a distance R_c from its BS is defined as the CC region. For the typical cell at the origin (referred to as 0-th cell hereafter), the CC region is given as

$$\begin{aligned}\mathcal{X}_C(\mathbf{o}, R_c, \Psi_b) &= \{\mathbf{x} \in \mathcal{V}_{\Psi_b}(\mathbf{o}) : \|\mathbf{x}\| \le R_c\} \\ &= \mathcal{V}_{\Psi_b}(\mathbf{o}) \cap \mathcal{B}_{R_c}(\mathbf{o}), \end{aligned} \tag{1}$$

where $\mathcal{V}_{\Psi_b}(\mathbf{o}) = \{\mathbf{x} \in \mathbb{R}^2 : \|\mathbf{x}\| \le \|\mathbf{x}-\mathbf{b}_j\|, \forall \mathbf{b}_j \in \Psi_b\}$ is the PVC associated with $\mathbf{b}_0$ and $\mathcal{B}_{R_c}(\mathbf{o})$ denotes a ball of radius R_c centered at $\mathbf{o}$. Note that the CC regions are equivalent to the JM cells associated with the BSs [28]. These JM cells are usually defined from the perspective of random nucleation and growth process. However, we follow (1) for simpler exposition. The region of the cell that is beyond R_c from the BS is the CE region and is given as

$$\mathcal{X}_E(\mathbf{o}, R_c, \Psi_b) = \{\mathbf{x} \in \mathcal{V}_{\Psi_b}(\mathbf{o}) : \|\mathbf{x}\| > R_c\}$$

$$= \mathcal{V}_{\Psi_b}(\mathbf{o}) \cap \mathcal{B}^C_{R_c}(\mathbf{o}). \quad (2)$$

The locations of the CC and CE users attached to the j-th BS are uniformly and randomly distributed within $\mathcal{X}_C(\mathbf{b}_j, R_c, \Psi_b)$ and $\mathcal{X}_E(\mathbf{b}_j, R_c, \Psi_b)$, respectively. We denote the CC area of the j-th cell as $X_{Cj}(\lambda_0, R_c) = |\mathcal{X}_C(\mathbf{b}_j, R_c, \Psi_b)|$ and the CE area as $X_{Ej}(\lambda_0, R_c) = |\mathcal{X}_E(\mathbf{b}_j, R_c, \Psi_b)|$. If the typical cell does not have a CE region, then $\mathcal{X}_E(\mathbf{b}_j, R_c, \Psi_b) = \varnothing$ and $X_{Ej}(\lambda_0, R_c) = 0$. Let N_{Cj} and N_{Ej} be the numbers of CC and CE users present in the j-th cell. We assume that both the random variables N_{Cj} and N_{Ej} follow zero-truncated Poisson distribution with parameters $\lambda_u X_{Cj}(\lambda_0, R_c)$ and $\lambda_u X_{Ej}(\lambda_0, R_c)$, respectively. Accordingly, conditioned on the CC (CE) area of the j-th cell, the PMFs of N_{Cj} and N_{Ej} for $n > 0$ are given as

$$\mathbb{P}\left[N_{Cj} = n | x_{cj}\right] = \frac{e^{-\lambda_u x_{cj}} (\lambda_u x_{cj})^n}{n!(1 - e^{-\lambda_u x_{cj}})},$$
$$\mathbb{P}\left[N_{Ej} = n | x_{ej}, \mathcal{E}_3^C\right] = \frac{e^{-\lambda_u x_{ej}} (\lambda_u x_{ej})^n}{n!(1 - e^{-\lambda_u x_{ej}})}, \quad (3)$$

where $\mathcal{E}_3^C$ is the event that the j-th cell has a CE region and is defined in Section III, x_{cj} and x_{ej} are the realizations of the CC and CE areas [1]. The main motivation behind consideration of the truncated Poisson distribution for users is to ensure that each BS in the network has at least one CC and CE user within its Voronoi cell. Since mMIMO will be primarily used for macro cells, from the system perspective, this is a reasonable assumption. Further, this allows us to model the user point process (to be defined shortly) as a Type-I process introduced in [26] facilitating a rigorous system analysis from the perspective of a typical cell. Note that λ_u is used to vary the load (number of users) in a cell.

Let us define a point process $\Psi_{\mathtt{u,CC}}$ that is constructed by randomly and uniformly distributing one point in the CC region of each cell. Mathematically, this can be expressed as

$$\Psi_{\mathtt{u,CC}} = \{U(\mathcal{X}_C(\mathbf{b}_j, R_c, \Psi_b)) : \forall \mathbf{b}_j \in \Psi_b\},$$

where $U(B)$ denotes a uniformly distributed point in $B \subset \mathbb{R}^2$. On the other hand, let Ψ_{bE} denote the set of BSs having a CE region that is defined as $\Psi_{bE} = \{\mathbf{b}_j : \forall \mathbf{b}_j \in \Psi_b, \mathcal{X}_E(\mathbf{b}_j, R_c, \Psi_b) \neq \varnothing\}$. Now, for the CE case we define the point process $\Psi_{\mathtt{u,CE}} = \{U(\mathcal{X}_E(\mathbf{b}_j, R_c, \Psi_b)) : \forall \mathbf{b}_j \in \Psi_{bE}\}$. Except the users attached to the BS at $\mathbf{o}$, rest of the users in the network belong to the interfering cells. Let the CC and CE point processes formed by the points in the interfering cells be

$$\Phi_{\mathtt{u,CC}} = \{U(\mathcal{X}_C(\mathbf{b}_j, R_c, \Psi_b)) : \forall \mathbf{b}_j \in \Phi_b\},$$
$$\Phi_{\mathtt{u,CE}} = \{U(\mathcal{X}_E(\mathbf{b}_j, R_c, \Psi_b)) : \forall \mathbf{b}_j \in \{\Psi_{bE} \setminus \mathbf{b}_0\}\}.$$

2) Pilot sequences: We restrict our analysis to a narrowband single-carrier system. Extension to a multi-carrier system is straightforward and hence is skipped in favour of simpler exposition. In order to get the CSI at the BS, in the j-th cell, each user is assigned a pilot (sequence) that is selected from a set of orthogonal pilots $\mathcal{P}_j \subset \mathcal{P}$, where $\mathcal{P} = \{\mathbf{p}_1, \mathbf{p}_2, \cdots, \mathbf{p}_B\}$ and $\mathbf{p}_i \in \mathbb{C}^{B \times 1}$ for $i = 1, 2, \ldots, B$, where B is the number of orthogonal pilots. Hence, the duration of each pilot sequence is B symbol duration. For convenience, we denote the pilots by their indices. Therefore, the set of indicies of the pilots used in the j-th cell is denoted as $\mathcal{K}_j \subset \mathcal{K}$, where $\mathcal{K} = \{1, 2, 3, \ldots, B\}$. Owing to the limited channel coherence time of T_c symbol duration, the cardinality of this set $|\mathcal{K}| = B \leq T_c$. While the pilots remain orthogonal in each cell, due to the consideration of FPR, orthogonality among cells is not guaranteed. In each cell, the pilots are partitioned into two different sets, i.e. for the j-th BS $\mathcal{K}_j = \mathcal{C} \cup \mathcal{E}_j$ where $\mathcal{C} = \{1, 2, \ldots, B_C\}$ contains the indices of the CC pilots that are reused in each cell. Moreover, $|\mathcal{C}| = B_C \leq B$. On the other hand, $\mathcal{E}_j$ contains the indices of the CE pilots used in the j-th cell, which are reused in other cells depending on the reuse factor β_f. Further, $|\mathcal{E}_j| = B_E$ and $(B - B_C)/\beta_f = B_E$ for all $\mathbf{b}_j \in \Psi_b$. The choice for B_C, B_E, and β_f is made such that all three are integers.

These pilots are assigned randomly to the user in a particular cell. For the k-th CC pilot sequence in the j-th cell, where $k \in \mathcal{C}$, we define a binary random variable $\mathcal{I}_{\mathtt{CC}}(j, k)$ as follows

$$\mathcal{I}_{\mathtt{CC}}(j,k) = \begin{cases} 1, & \text{if } k\text{-th CC pilot is used in the } j\text{-th cell,} \\ 0, & \text{if } k\text{-th CC pilot is not used in the } j\text{-th cell.} \end{cases} \quad (4)$$

On the similar lines, for the l-th CE pilot in the j-th cell, we define the binary random variable $\mathcal{I}_{\mathtt{CE}}(j, l)$. Let $\Phi^{\mathtt{CC}}_{\mathtt{u,k}}$ and $\Phi^{\mathtt{CE}}_{\mathtt{u,l}}$ be the point processes formed by the interfering CC and CE users that use the k-th CC and l-th CE pilots, respectively. Since the user locations in $\Phi^{\mathtt{CC}}_{\mathtt{u,k}}$ are uniformly distributed points in the CC region of their respective cells, $\Phi^{\mathtt{CC}}_{\mathtt{u,k}}$ can be defined to inherit the user locations from $\Phi_{\mathtt{u,CC}}$ when $\mathcal{I}_{\mathtt{CC}}(j, k) = 1$. Similar argument is true for $\Phi^{\mathtt{CE}}_{\mathtt{u,l}}$ and $\Phi_{\mathtt{u,CE}}$. Hence,

$$\Phi^{\mathtt{CC}}_{\mathtt{u,k}} = \{\mathbf{u} : \mathbf{u} \in \Phi_{\mathtt{u,CC}}, \mathcal{I}_{\mathtt{CC}}(j,k) = 1\}, \text{and}$$
$$\Phi^{\mathtt{CE}}_{\mathtt{u,l}} = \{\mathbf{u} : \mathbf{u} \in \Phi_{\mathtt{u,CE}}, \mathcal{I}_{\mathtt{CE}}(j,l) = 1\}. \quad (5)$$

We defer the discussion on the statistical properties of these point processes to Section V. Note that the point process formed by the users using other pilot sequences in the network can be defined on the similar lines as that of $\Phi^{\mathtt{CC}}_{\mathtt{u,k}}(\Phi^{\mathtt{CE}}_{\mathtt{u,l}})$, where the points will be inherited from a point process that has the same definition as $\Phi_{\mathtt{u,CC}}(\Phi_{\mathtt{u,CE}})$. In the illustrative network diagram (Fig. 1), one CC pilot that is reused in each cell and one CE pilot that is reused in a few of the cells.

3) Distance distributions: Let the location of the user that uses the k-th sequence in the j-th cell be denoted as $\mathbf{u}_{j_k}$. The random distance between a user at $\mathbf{u}_{j_k}$ and a BS at $\mathbf{b}_i$ is denoted by the random variable $D_{ij_k} = \|\mathbf{u}_{j_k} - \mathbf{b}_i\|$ and d_{ij_k} is its realization. To obtain the coverage probability of a randomly selected user CC (CE) user, we need the distribution of the serving distance D_{00_k} (D_{00_l}) between $\mathbf{b}_0$ and the CC (CE) user using the k-th (l-th) pilot in the 0-th cell. For a typical PVC, the distance distribution between the BS and a randomly located point in the PVC is approximated as Rayleigh distribution with scale parameter $(\sqrt{2\pi\lambda_0 c_2})^{-1}$, where $c_2 = 5/4$ is an empirically obtained correction fac-

[1]Throughout this manuscript, we have represented a random variable in capital letter and its realization in small letter.

TABLE I: Summary of Notations

Notation	Description
Ψ_b and λ_0	Homogeneous PPP modeling the locations BSs and density of Ψ_b
$\mathbf{b}_j$ and $\mathbf{u}_{j_k}$	Locations of the j-th BS and a user in the j-th cell using k-th pilot
R_c and $\kappa = R_c\sqrt{\pi c_2 \lambda_0}$	Threshold radius and normalized threshold radius
$\mathcal{V}_{\Psi_b}(\mathbf{b}_j)$	Voronoi cell associated with the j-th BS
$\mathcal{X}_C(\mathbf{b}_j, R_c, \Psi_b)$ and $\mathcal{X}_E(\mathbf{b}_j, R_c, \Psi_b)$	CC and CE region of the j-th cell
$X_{Cj}(\lambda_0, R_c)$ and $X_{Ej}(\lambda_0, R_c)$	CC and CE areas of a typical cell in a network of BS density λ_0
$\Phi^{\mathtt{CC}}_{\mathtt{u},\mathtt{k}}$ and $\lambda^{\mathtt{CC}}_{\mathtt{u},\mathtt{k}}(r,\kappa)$	Point processes of users using k-th CC pilot and its density function
$\mathcal{I}_{\mathtt{CC}}(j,k), \mathcal{I}_{\mathtt{CE}}(j,l)$	Indicator variable that is 1 when k-th CC pilot, l-th CE pilot is used in j-th cell
$\mathcal{A}_{0,\mathtt{CC}}$ ($\mathcal{A}_{0,\mathtt{CE}}$)	Indicator variable for pilot assignment to CC (CE) user of interest
$\mathcal{A}_{\mathtt{0n},\mathtt{CC}}$ ($\mathcal{A}_{\mathtt{0m},\mathtt{CE}}$)	Indicator variable for n-th (m-th) pilot assignment to CC (CE) user
D_{ij_k}	Random distance between the BS at $\mathbf{b}_j$ and user at $\mathbf{u}_{j_k}$
$\mathbf{g}_{ij_k} \sim \mathcal{CN}(\mathbf{0}_M, d_{ij_k}^{-\alpha}\mathbf{I}_M)$	Channel vector between i-th BS and the user at $\mathbf{u}_{j_k}$
$\mathtt{SINR}_{0_k}$	SINR of the user using the k-th pilot in the 0-th cell
$\mathtt{P}^{\mathtt{CC}}_{\mathtt{c},\mathtt{k}}$ and $\mathtt{P}^{\mathtt{CE}}_{\mathtt{c},\mathtt{l}}$	Coverage probability of a user using k-th CC and l-th CE pilots
B, B_C, and B_E	Total number of pilots, number of CC, and number of CE pilots
T_c, B	Length of coherence time and pilot sequence (in symbol durations)

tor [29]. Since the user at $\mathbf{u}_{0_k}$ can not lie beyond $\mathcal{B}_{R_c}(\mathbf{o})$, it is reasonable to approximate the distribution of D_{00_k} to follow truncated Rayleigh distribution as given below

$$F_{D_{00_k}}(d_{00_k}|R_c) = \frac{1-\exp(-\pi c_2 \lambda_0 d_{00_k}^2)}{1-\exp(-\pi c_2 \lambda_0 R_c^2)}, \quad d_{00_k} \leq R_c. \tag{6}$$

On the other hand, the distribution of distance D_{00_l} can also be approximated as

$$F_{D_{00_l}}(d_{00_l}|R_c) = 1-\exp(-\pi c_2 \lambda_0 (d_{00_l}^2 - R_c^2)), \quad d_{00_l} > R_c. \tag{7}$$

At this point, in order to make R_c invariant to the BS density λ_0, we define a normalized radius κ as $R_c = \frac{\kappa}{\sqrt{\pi c_2 \lambda_0}}, \kappa \in [0,\infty)$. In Sec. V, κ will be used in the statistical characterization of $\Phi^{\mathtt{CC}}_{\mathtt{u},\mathtt{k}}(\Phi^{\mathtt{CE}}_{\mathtt{u},\mathtt{l}})$. Further, κ also provides perspective regarding the size of the CC region without the knowledge of λ_0. Next, we define the system parameters from the perspective of the CC user using the k-th pilot sequence. The extension of these definitions for CE case is straightforward.

B. Channel model and channel estimation

1) Channel model: We consider a system where each link suffers from two multiplicative wireless channel impairments, namely distance-dependent pathloss and multi-path fading. Consideration of the effect of shadowing is left as a promising future work. The channel vector between the user located at $\mathbf{u}_{j_k}$ and the M antenna elements of the BS located at $\mathbf{b}_i$ is given as $\mathbf{g}_{ij_k} = d_{ij_k}^{-\alpha/2}\mathbf{h}_{ij_k} (\in \mathbb{C}^{M\times 1})$, where α is the pathloss exponent, $\mathbf{h}_{ij_k} \sim \mathcal{CN}(\mathbf{0}_M, \mathbf{I}_M)$ is a $M \times 1$ complex Gaussian vector. We assume that these channel vectors exhibit quasi-orthogonality, i.e.

$$\lim_{M\to\infty} \frac{1}{M}\mathbf{h}_{ij_m}^H \mathbf{h}_{ij_n} = \mathbf{1}(j_m = j_n). \tag{8}$$

Further, we consider user transmit power ρ_u to be fixed for both pilot and data symbols.

2) Channel estimation: In a cell, using the orthogonal pilots, corresponding BS obtains the least square channel estimate of the users attached to them. Hence, for the CC user using the k-th pilot, the channel estimate at the 0-th BS is given as $\tilde{\mathbf{g}}_{00_k} = \sqrt{\rho_u}\mathbf{g}_{00_k} + \sum_{\mathbf{u}_{j_k}\in\Phi_{\mathtt{u},\mathtt{k}}} \sqrt{\rho_u}\mathbf{g}_{0j_k} + \mathbf{v}_0 \in \mathbb{C}^{M\times 1}$, where $\mathbf{v}_0 \sim \mathcal{CN}(\mathbf{0}_M, \mathbf{I}_M)$ is a complex Gaussian noise vector.

C. Asymptotic UL SINR *of a CC (CE) user assigned to k-th (l-th) pilot sequence*

The received signal vector at the 0-th BS is given as

$$\mathbf{r}_0 = \mathbf{h}_{00_k} x_{0k} d_{00_k}^{-\alpha/2} + \sum_{i=1, i\neq k}^{B} \mathcal{I}_{\mathtt{CC}}(0,i)\mathbf{h}_{00_i} x_{0i} d_{00_i}^{-\alpha/2} + \sum_{i=1}^{B}\sum_{\mathbf{u}_{j_i}\in\Phi^{\mathtt{CC}}_{\mathtt{u},\mathtt{i}}} \mathbf{h}_{0j_i} x_{ji} d_{0j_i}^{-\alpha/2} + \mathbf{n}_0, \tag{9}$$

where x_{ji} is the data symbol transmitted by the user using the i-th pilot in the j-th cell, $\mathbf{n}_0 \sim \mathcal{CN}(\mathbf{0}_M, \mathbf{I}_M)$ is a complex Gaussian noise vector. We assume that $\mathbb{E}[x_{ji}] = 0$ and $\mathbb{E}\left[\|x_{ji}\|^2\right] = \rho_u$. In order to estimate the symbol transmitted by the CC user of interest, the 0-th BS uses MRC detection scheme, where the filter coefficients are given as $\mathbf{w}_{0_k} = \frac{1}{M}\tilde{\mathbf{g}}_{00_k}^H$. As demonstrated in various works in the literature (cf. [30]), the asymptotic SINR of a user is independent of the detection scheme. Now, the detected symbol for the CC user using the k-th pilot in the 0-th BS is given as $\hat{x}_{0k} = \mathbf{w}_{0_k}\mathbf{r}_0$. As the number of antennas $M \to \infty$, due to quasi-orthogonality of the channel, it can be shown that the detected symbol is only affected by the interference from the users using the k-th pilot in other cells (a.k.a. pilot contamination). Hence, the SINR of the CC and CE users that are assigned the k-th and l-th pilots, respectively, are given as

$$\mathtt{SINR}_{0_k} = d_{00_k}^{-2\alpha}\Bigg(\sum_{\mathbf{u}_{j_k}\in\Phi^{\mathtt{CC}}_{\mathtt{u},\mathtt{k}}} d_{0j_k}^{-2\alpha}\Bigg)^{-1}, \text{and}$$

$$\mathtt{SINR}_{0_l} = d_{00_l}^{-2\alpha}\Bigg(\sum_{\mathbf{u}_{j_l}\in\Phi^{\mathtt{CE}}_{\mathtt{u},\mathtt{l}}} d_{0j_l}^{-2\alpha}\Bigg)^{-1}. \tag{10}$$

The proof of the above SINR expression is readily available in the literature (cf. [2], [18]). Since the above expressions are independent of ρ_u, we assume $\rho_u \equiv 1$.

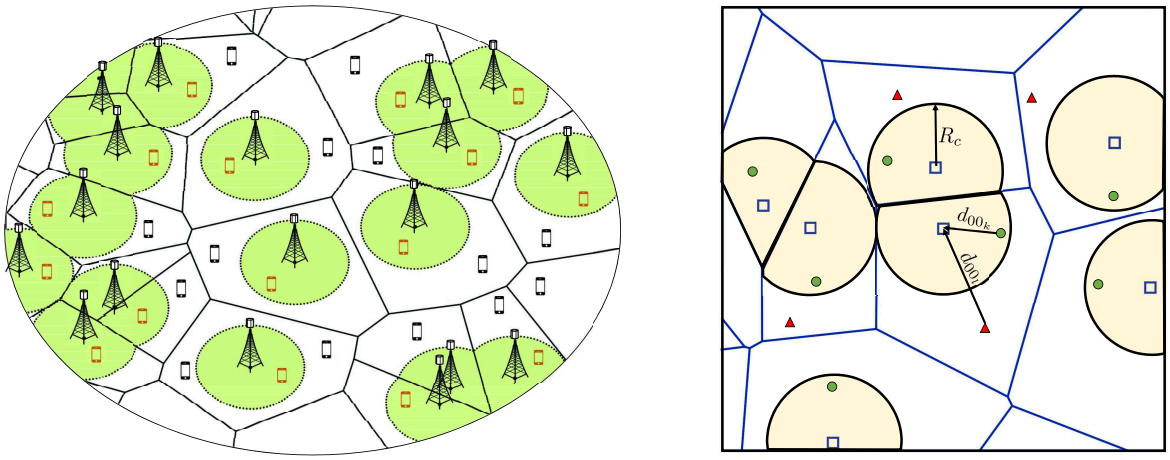

Fig. 1: A representative network diagram (left) and a network realization illustrating the users using the k-th CC and l-th CE pilot (right). In a few of the cells the CE pilot is not in use.

D. Performance metrics

In this work, the following metrics are considered for the network performance analysis.

1) $\mathtt{SINR}$ *coverage probability:* The $\mathtt{SINR}$ coverage probabilities of a CC and CE user using the k-th and l-th pilots for a target $\mathtt{SINR}$ threshold T are

$$\mathtt{P}_{\mathtt{c,k}}^{\mathtt{CC}}(T) = \mathbb{P}\left[\mathtt{SINR}_{0_k} \geq T | \mathcal{I}_{\mathtt{CC}}(0,k) = 1\right], \text{and}$$
$$\mathtt{P}_{\mathtt{c,l}}^{\mathtt{CE}}(T) = \mathbb{P}\left[\mathtt{SINR}_{0_l} \geq T | \mathcal{I}_{\mathtt{CE}}(0,l) = 1, \mathcal{E}_3^C\right].$$

2) Average user SE: The average user SEs of the CC and CE users of interest are given as

$$\overline{\mathtt{SE}}_{\mathtt{u,CC}} = \omega \mathbb{E}\left[\mathcal{A}_{0,\mathtt{CC}} \log_2(1 + \mathtt{SINR}_{0,\mathtt{CC}})\right], \text{and}$$
$$\overline{\mathtt{SE}}_{\mathtt{u,CE}} = \omega \mathbb{E}\left[\mathcal{A}_{0,\mathtt{CE}} \log_2(1 + \mathtt{SINR}_{0,\mathtt{CE}}) \middle| \mathcal{E}_3^C\right], \tag{11}$$

where $\omega = (1 - B/T_c)$ accounts for the fact that out of the total coherence time of T_c symbol duration, B symbol duration is dedicated for channel estimation leaving only $T_c - B$ duration for data transmission. Note that while the coverage probability is defined for a user conditioned on a pilot, the average user SE is defined for a randomly selected CC (CE) user that can be assigned any one of the CC (CE) pilots. Hence, $\mathtt{SINR}_{0,\mathtt{CC}}$ and $\mathtt{SINR}_{0,\mathtt{CE}}$ is the $\mathtt{SINR}$ of a randomly selected CC (CE) user that we term as *CC (CE) user of interest*. Further, the indicator variable $\mathcal{A}_{0,\mathtt{CC}} = 1$, if the CC user of interest is assigned a pilot sequence, and $\mathcal{A}_{0,\mathtt{CC}} = 0$, otherwise. Similarly, we define the indicator variable $\mathcal{A}_{0,\mathtt{CE}}$ for a random CE user of interest.

3) Average cell SE: The cell SE of the 0-th cell is given as

$$\mathtt{CSE} = \omega \Bigg[\sum_{n=1}^{B_C} \mathcal{I}_{\mathtt{CC}}(0,n) \log_2(1 + \mathtt{SINR}_{0_n}) + \sum_{m=1}^{B_E} \mathcal{I}_{\mathtt{CE}}(0,m) \log_2(1 + \mathtt{SINR}_{0_m}) \Bigg], \tag{12}$$

where $\omega = (1 - B/T_c)$. Our metric of interest is $\mathbb{E}\left[\mathtt{CSE}\right]$. In the following sections, we derive theoretical expressions for the aforementioned quantities.

III. Distributions of the CC and CE areas of a typical cell

As discussed in the previous section, the distribution of the number of CC (CE) users and subsequently the pilot utilization in an interfering cell depends on its CC (CE) area. Since exact characterization of CE area is challenging (it is an open problem), we provide an approximate area distribution for the CE area using the well-known Weibull distribution. In our approach, we first derive the exact expressions for the first two moments of the CE area of a typical cell. In the second step, using moment matching method, we approximate this area as Weibull distribution. We use the similar method to approximate the CC area distributions as a truncated beta distribution. While the exact characterization of the distribution of a typical JM cell area, hence the CC area, is given in [31], the expression of the probability density function (PDF) involves an infinite summation over multi-dimensional integrations. Further, the order of integration (hence the complexity of the expression) increases with the increasing value of R_c. Hence, our approximate truncated beta distribution lends tractability to the analysis. We validate the accuracy of the proposed distributions through Monte Carlo simulations using statistical metrics such as Kulback-Leibler divergence (KLD) and Kolmogorov-Smirnov distance (KSD). It is worth mentioning that the area of a typical PVC is approximated to follow gamma distribution, whose properties are used to provide load-based analysis of cellular networks [32], [33].

A. Distribution of CE area of a typical cell

To begin with, in the following lemma, we present the first two moments of the CE area.

Lemma 1. *For a given R_c and λ_0, the mean CE area of a typical Voronoi cell is*

$$m_{1,X_{E0}}(\lambda_0, R_c) = \mathbb{E}\left[X_{E0}(\lambda_0, R_c)\right] = \frac{\exp(-\pi\lambda_0 R_c^2)}{\lambda_0}, \tag{13}$$

and the second moment of the area is $m_{2,X_{E0}}(\lambda_0, R_c) = \mathbb{E}\left[X_{E0}(\lambda_0, R_c)^2\right]$

$$=2\pi \int_{r_1=R_c}^{\infty} \int_{r_2=R_c}^{\infty} \int_{u=0}^{2\pi} \exp\left(-\lambda_0 V(r_1,r_2,u)\right) \mathrm{d}u r_2 \mathrm{d}r_2 r_1 \mathrm{d}r_1, \tag{14}$$

where $V(r_1,r_2,u)$ is the area of union of two circles. The radii of these circles are r_1 and r_2, and the angular separation between their centers with respect to origin is u. Further, $V(r_1,r_2,u) =$

$$r_1^2\left(\pi - v(r_1,r_2,u) + \frac{\sin(2v(r_1,r_2,u))}{2}\right) + r_2^2\left(\pi - w(r_1,r_2,u) + \frac{\sin(2w(r_1,r_2,u))}{2}\right), \tag{15}$$

where $v(r_1,r_2,u) = \cos^{-1}\left(\frac{r_1 - r_2\cos(u)}{\sqrt{r_1^2+r_2^2-2r_1r_2\cos(u)}}\right)$, *and* $w(r_1,r_2,u) = \cos^{-1}\left(\frac{r_2 - r_1\cos(u)}{\sqrt{r_1^2+r_2^2-2r_1r_2\cos(u)}}\right)$.

Proof: Please refer to Appendix A. ∎

Before proceeding further, some intuition on the type of distribution that provides an accurate approximation is necessary. Note that a Voronoi cell has two characteristic radii R_m and R_M [34]. While R_m corresponds to the radius of the largest circle that completely lies inside a Voronoi cell, R_M is the radius of the smallest circle that encircles a Voronoi cell. Using R_m and R_M, we define following three disjoint events: (i) $\mathcal{E}_1 = \{R_c < R_m\}$, i.e. the CC region completely lies inside the Voronoi cell, (ii) $\mathcal{E}_2 = \{R_m \le R_c < R_M\}$, i.e. the circle $\mathcal{B}_{R_c}(\mathbf{o})$ and the Voronoi cell $\mathcal{V}_{\Psi_b}(\mathbf{o})$ intersects, and (iii) $\mathcal{E}_3 = \{R_M \le R_c\}$, i.e. there is no CE region. So, the CE area PDF can be expressed as the sum of two components:

$$f_{X_{E0}}(x) = f_{X_{E0}}(x|\mathcal{E}_3)\mathbb{P}\left[\mathcal{E}_3\right] + f_{X_{E0}}(x|\mathcal{E}_3^C)(1-\mathbb{P}\left[\mathcal{E}_3\right]), \tag{16}$$

Further, note that $f_{X_{E0}}(x|\mathcal{E}_3)$ is given as

$$f_{X_{E0}}(x|\mathcal{E}_3) = \delta(0), \tag{17}$$

where $\delta(x)$ is the Dirac-delta function. Next we obtain $\mathbb{P}\left[\mathcal{E}_3\right]$ and $f_{X_{E0}}(x|\mathcal{E}_3)$. Since $\mathcal{E}_3 = \{R_M \le R_c\}$, $\mathbb{P}\left[\mathcal{E}_3\right] = \mathbb{P}\left[R_M \le R_c\right]$, where the distribution of R_M is [34, Theorem 1]

$$\mathbb{P}\left[R_M \le r\right] = 1 - e^{-4\pi\lambda_0 r^2}\left(1 - \sum_{k\ge 1}\frac{(-4\pi\lambda_0 r^2)^k}{k!}\xi_k\right), \quad r>0. \tag{18}$$

In the above expression,

$$\xi_k = \int_{\sum_{i=1}^{k} u_i = 1, u_i\in[0,1]} \left[\prod_{i=1}^{k} F(u_i)\right] e^{4\pi\lambda_0 r^2 \sum_{i=1}^{k}\int_0^{u_i} F(t)\mathrm{d}t}\mathrm{d}\mathbf{u},$$

where $F(t) = \sin^2(\pi t)\mathbf{1}(0\le t\le \frac{1}{2}) + \mathbf{1}(t>\frac{1}{2})$, where $\mathbf{1}(\cdot)$ is the indicator function. Based on moment matching method, we approximate $f_{X_{E0}}(x|\mathcal{E}_3^C)$ as Weibull PDF. Intuitively, the CE area is likely to exhibit similar properties of the Voronoi cell area, especially when R_c is small. Hence, the gamma distribution, which is used to approximate the Voronoi cell area, is the first preference. However, for larger R_c, gamma PDF fails to capture the decay of the PDF of CE area. Hence, Weibull distribution, which has similar Kernel as gamma distribution[2] along with the flexibility to control the decay factor of the PDF, is used for the aforementioned approximation. Now, we present the mean and variance of X_{E0} conditioned on $\mathcal{E}_3^C$.

Lemma 2. *The mean and variance of the CE area conditioned on $\mathcal{E}_3^C$ are*

$$\mathbb{E}\left[X_{E0}|\mathcal{E}_3^C\right] = \mathbb{E}\left[X_{E0}\right](\mathbb{P}\left[\mathcal{E}_3^C\right])^{-1} \text{ and}$$
$$\mathtt{Var}\left[X_{E0}|\mathcal{E}_3^C\right] = \frac{\mathtt{Var}\left[X_{E0}\right]}{\mathbb{P}\left[\mathcal{E}_3^C\right]} - \mathbb{P}\left[\mathcal{E}_3\right](\mathbb{E}\left[X_{E0}|\mathcal{E}_3^C\right])^2.$$

Proof: The proof of this Lemma follows from law of total expectation and law of total variance that are given as $\mathbb{E}\left[X_{E0}\right] = \mathbb{E}\left[X_{E0}|\mathcal{E}_3\right]\mathbb{P}\left[\mathcal{E}_3\right] + \mathbb{E}\left[X_{E0}|\mathcal{E}_3^C\right]\mathbb{P}\left[\mathcal{E}_3^C\right]$, and

$$\begin{aligned}\mathtt{Var}\left[X_{E0}\right] =& \mathtt{Var}\left[X_{E0}|\mathcal{E}_3\right]\mathbb{P}\left[\mathcal{E}_3\right] \\ &+ \mathbb{P}\left[\mathcal{E}_3\right](1-\mathbb{P}\left[\mathcal{E}_3\right])(\mathbb{E}\left[X_{E0}|\mathcal{E}_3\right])^2 \\ &+ \mathtt{Var}\left[X_{E0}|\mathcal{E}_3^C\right]\mathbb{P}\left[\mathcal{E}_3^C\right] \\ &+ \mathbb{P}\left[\mathcal{E}_3^C\right]\mathbb{P}\left[\mathcal{E}_3\right](\mathbb{E}\left[X_{E0}|\mathcal{E}_3^C\right])^2 \\ &- 2\mathbb{E}\left[X_{E0}|\mathcal{E}_3\right]\mathbb{P}\left[\mathcal{E}_3\right]\mathbb{E}\left[X_{E0}|\mathcal{E}_3^C\right]\mathbb{P}\left[\mathcal{E}_3^C\right].\end{aligned}$$

Rearranging the terms and replacing $\mathbb{E}\left[X_{E0}|\mathcal{E}_3\right] = 0$ and $\mathtt{Var}\left[X_{E0}|\mathcal{E}_3\right] = 0$, we obtain the expressions presented in the lemma. ∎

The conditional PDF of X_{E0} is given as

$$f_{X_{E0}}(x|\mathcal{E}_3^C) = \frac{\eta}{\zeta}\left(\frac{x}{\zeta}\right)^{\eta-1}\exp\left(-\frac{x^\eta}{\zeta^\eta}\right), \tag{19}$$

where η and ζ are shape and scale parameters. These parameters are obtained by matching the first two moments and solving the following system of equations:

$$\begin{aligned}\eta\Gamma(1+1/\zeta) &= \mathbb{E}\left[X_{Ej}|\mathcal{E}_3^C\right], \\ \eta^2(\Gamma(1+2/\zeta) - \Gamma(1+1/\zeta)^2) &= \mathtt{Var}\left[X_{Ej}|\mathcal{E}_3^C\right].\end{aligned} \tag{20}$$

Now, (19), (18), (17), and (16) together provide us the approximate PDF for CE area.

B. Distribution of CC area of a typical cell

Similar to the CE case, in the next lemma, we derive the first two moments of the CC area.

Lemma 3. *For a given λ_0 and R_c, the mean of the CC area a typical Voronoi cell is given by*

$$m_{1,X_{C0}}(\lambda_0,R_c) = \mathbb{E}\left[X_{C0}(\lambda_0,R_c)\right] = \frac{1-\exp(-\pi\lambda_0 R_c^2)}{\lambda_0}, \tag{21}$$

and the second moment of the area is given by $m_{2,X_{E0}}(\lambda_0,R_c) =$

$$\mathbb{E}\left[X_{C0}(\lambda_0,R_c)^2\right] = 2\pi\int_{r_1=0}^{R_c}\int_{r_2=0}^{R_c}\int_{u=0}^{2\pi} e^{-\lambda_0 V(r_1,r_2,u)}\mathrm{d}u r_2\mathrm{d}r_2 r_1\mathrm{d}r_1, \tag{22}$$

[2]The kernel of gamma PDF is $f_G(x)\propto x^{\xi-1}\exp(-x/\theta)$, and Weibull PDF is $f_W(x)\propto x^{\xi-1}\exp(-(x/\theta)^\xi)$.

where $V(r_1, r_2, u)$ is the area of union of two circles given in (15).

Proof: On the similar lines of the proof of Lemma 1, the mean CC area of the 0-th cell is

$$\mathbb{E}\left[|\mathcal{X}_C(\mathbf{o}, R_c, \Psi_b)|\right] = 2\pi \int_{r=0}^{R_c} \exp(-\pi\lambda_0 r^2) r \mathrm{d}r.$$

Similarly, the second moment of the j-th CC area is given as

$$\mathbb{E}\left[|\mathcal{X}_C(\mathbf{o}, R_c, \Psi_b)|^2\right] = \mathbb{E}\Big[\int_{\mathbf{x}\in\mathbb{R}^2} \mathbf{1}_{(\mathbf{x}\in\mathcal{V}_{\Psi_b}(\mathbf{o})\cap\mathcal{B}_{R_c}(\mathbf{o}))}\mathrm{d}\mathbf{x} \int_{\mathbf{y}\in\mathbb{R}^2} \mathbf{1}_{(\mathbf{y}\in\mathcal{V}_{\Psi_b}(\mathbf{o})\cap\mathcal{B}_{R_c}(\mathbf{o}))}\mathrm{d}\mathbf{y}\Big],$$

On the similar lines as in Appendix A, after a few steps (22) follows from the above expression. ∎

Now, the PDF of the CC area can be expressed as

$$f_{X_{C0}}(x) = f_{X_{C0}}(x|\mathcal{E}_1)\mathbb{P}\left[\mathcal{E}_1\right] + f_{X_{C0}}(x|\mathcal{E}_1^C)(1-\mathbb{P}\left[\mathcal{E}_1\right]), \tag{23}$$

where $\mathbb{P}\left[\mathcal{E}_1\right] = \mathbb{P}\left[R_m > R_C\right]$. Note that R_m is half of the nearest neighbor distance of a PPP, which follows Rayleigh distribution with parameter $(\sqrt{8\pi\lambda_0})^{-1}$ and CDF $F_{R_m}(r_m) = 1-\exp(-4\pi\lambda_0 r_m^2)$. Hence, the probability of $\mathcal{E}_1$ is given as

$$\mathbb{P}\left[\mathcal{E}_1\right] = \mathbb{P}\left[R_m > R_c\right] = \exp(-4\pi\lambda_0 R_c^2) = 1-\mathbb{P}\left[\mathcal{E}_1^C\right]. \tag{24}$$

Observe that, the PDF of X_{C0} conditioned on $\mathcal{E}_1$ is

$$f_{X_{C0}}(x|\mathcal{E}_1) = \delta(\pi R_c^2). \tag{25}$$

Now, to approximate $f_{X_{C0}}(x|\mathcal{E}_1^C)$, we have used generalized truncated beta distribution, i.e.

$$f_{X_{C0}}(x|\mathcal{E}_1^C) \approx g(x; v, w, y, z, \gamma, \beta) = \frac{(x-y)^{\gamma-1}(z-x)^{\beta-1}}{B(v, w, y, z; \gamma, \beta)}, \quad 0 \le x < \pi R_c^2, \tag{26}$$

where γ and β are shape parameters; the support of the untruncted beta distribution is $[y, z]$ (since beta distribution has finite support); the support of the truncated beta distribution is $[v, w]$; and the normalization factor $B(v, w, y, z; \gamma, \beta) = \int_{\mathfrak{v}}^{\mathfrak{w}} (x-y)^{\gamma-1}(z-x)^{\beta-1}\mathrm{d}x$, where $\mathfrak{v} = \frac{v-y}{y-z}$ and $\mathfrak{w} = \frac{w-y}{z-y}$. The choice of beta distribution is motivated by the fact that the distribution function of X_{C0} has a finite support $[0, \pi R_c^2]$. Based on this support set, we set $v = 0$ and $w = \pi R_c^2$ for the PDF presented in (26). Another motivation behind selection of beta is the presence of an additional shape parameter compared to conventional distributions such as Gamma or Weibull, which are parametrized by a single shape parameter. Further, we are introducing truncation to the above distribution that gives us an additional degree of freedom to closely match any arbitrary shape of the actual PDF. Here, we set $y = 0$ and $z = 3/2\pi R_c^2$. To obtain the shape parameters γ and β using moment matching method, we need the mean and variance of X_{C0} conditioned on $\mathcal{E}_1^C$, which is presented next.

Lemma 4. *The mean and variance of the area X_{C0} conditioned on $\mathcal{E}_1^C$ is given as*

$$\mathbb{E}\left[X_{C0}|\mathcal{E}_1^C\right] = \frac{(1-e^{-\pi\lambda_0 R_c^2})\lambda_0^{-1} - \pi R_c^2 e^{-4\pi\lambda_0 R_c^2}}{1-e^{-4\pi\lambda_0 R_c^2}},$$

$$\mathtt{Var}\left[X_{C0}|\mathcal{E}_1^C\right] = \frac{\mathtt{Var}\left[X_{C0}\right]}{\mathbb{P}\left[\mathcal{E}_1^C\right]} - \mathbb{P}\left[\mathcal{E}_1\right]\left(\mathbb{E}\left[X_{C0}|\mathcal{E}_1\right] - \mathbb{E}\left[X_{C0}|\mathcal{E}_1^C\right]\right)^2. \tag{27}$$

Proof: The proof is done on the similar lines as that of Lemma 2. Using the law of total expectation, we write

$$\mathbb{E}\left[X_{C0}|\mathcal{E}_1^C\right] = \left(\mathbb{E}\left[X_{C0}\right] - \mathbb{E}\left[X_{C0}|\mathcal{E}_1\right]\mathbb{P}\left[\mathcal{E}_1\right]\right)/(1-\mathbb{P}\left[\mathcal{E}_1\right]).$$

The mean of the conditional area in the Lemma is obtained by substituting $\mathbb{E}\left[X_{C0}|\mathcal{E}_1\right] = \pi R_c^2, \mathbb{P}\left[\mathcal{E}_1\right] = e^{-4\pi\lambda_0 R_c^2}$, and using the value of $\mathbb{E}\left[X_{C0}\right]$ from Lemma 3. Further, the conditional variance is obtained from the law of total variance and using the fact that $\mathtt{Var}\left[X_{C0}|\mathcal{E}_1\right] = 0$. ∎

The parameters γ, β in (26) are obtained by solving the following simultaneous equations

$$\frac{\mathtt{B}(v, w, y, z; \gamma+1, \beta)}{\mathtt{B}(v, w, y, z; \gamma, \beta)} = \mathbb{E}\left[X_{C0}|\mathcal{E}_1^C\right],$$

$$\frac{\mathtt{B}(v, w, y, z; \gamma+2, \beta)}{\mathtt{B}(v, w, y, z; \gamma, \beta)} - \mathbb{E}\left[X_{C0}|\mathcal{E}_1^C\right]^2 = \mathtt{Var}\left[X_{C0}|\mathcal{E}_1^C\right].$$

Substituting (24) and (25) in (23), the approximate CC area PDF is given as

$$f_{X_{C0}}(x) = \delta(\pi R_c^2)e^{-4\pi\lambda_0 R_c^2} + f_{X_{C0}}(x|\mathcal{E}_1^C)(1-e^{-4\pi\lambda_0 R_c^2}), \tag{28}$$

where $f_{X_{C0}}(x|\mathcal{E}_1^C)$ is given in (26).

Remark 1. *It is possible to approximate the* PDF *of the area of a typical Voronoi cell using the expressions for $f_{X_{C0}}(x)$ in* (16) *or $f_{X_{C0}}(x)$ in* (28)*. While in the former case, the typical Voronoi cell area* PDF *is obtained by setting $R_c = 0$, in the latter case it is obtained by setting a sufficiently large value of R_c such that $\mathbb{P}\left[\mathcal{E}_1\right] = \exp(-\pi\lambda_0 R_c^2) \approx 0$.*

C. Accuracy of the approximate distributions

The approximate theoretical results are validated through Monte Carlo simulations. We use KLD (KSD) to compare the approximate and the true PDFs (CDFs) obtained through simulations. In Table II these two metrics are presented for different values of R_c for both CC and CE areas. The low values of KSD and KLD for different R_c verifies the accuracy of the distributions. For visual verification, in Fig. 2, we compare the true and approximate PDFs of CC and CE areas.

IV. Pilot Assignment and Pilot Utilization Probability

In this section, we present theoretical expressions for the probability of assigning a pilot to the CC (CE) user of interest (Lemma 5) and the probability that the k-th CC (l-th CE) pilot is being used in the j-th cell (Lemma 6). As we will see in the following section, the former quantity is useful in obtaining the average SE of the CC (CE) user of interest, and the latter quantity is useful in determining the average cell

$R_c \vert \kappa$	100|0.4	200|0.8	250|1	300|1.2	500|2
KS Distance (CC)	0.0230	0.0238	0.0123	0.0104	0.002
KL Divergence (CC)	0.0125	0.0095	0.0055	0.0032	0.0007
KS Distance (CE)	0.0164	0.0107	0.0233	0.0347	
KL Divergence (CE)	0.0098	0.0087	0.0160	0.0208	

TABLE II: Comparison between simulation and approximate PDFs and CDFs for different R_c. $\lambda_0 = 4 \times 10^{-6}$.

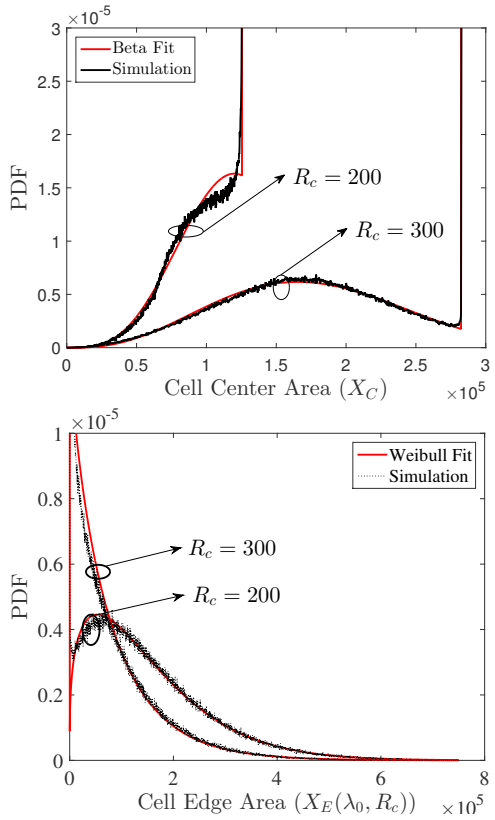

Fig. 2: The PDFs (top) of the CC area and CE area (bottom) of a typical cell. $\lambda_0 = 4 \times 10^{-6}$.

SE as well as the density function of interfering CC (CE) user point process. Before proceeding further, let us define the binary variable $\mathcal{A}_{\mathtt{0n,CC}} = 1$, if the CC user of interest is assigned the n-th pilot sequence, and $\mathcal{A}_{\mathtt{0n,CC}} = 0$, otherwise. Similarly, the indicator variable $\mathcal{A}_{\mathtt{0m,CE}}$ can be defined for CE user of interest and the m-th CE pilot. Next, we present the probability of pilot assignment to the CC (CE) user of interest.

Lemma 5. *The probability that CC user of interest is assigned the k-th pilot is*

$$\mathbb{E}\left[\mathcal{A}_{\mathtt{0k,CC}}\right] = \mathbb{P}\left[\mathcal{A}_{\mathtt{0k,CC}} = 1\right] = B_C^{-1}\mathbb{P}\left[\mathcal{A}_{\mathtt{0,CC}} = 1\right]$$
$$= B_C^{-1} \int_0^{\pi R_c^2} \mathbb{P}\left[\mathcal{A}_{\mathtt{0,CC}} = 1 | x_{c0}\right] f_{X_{C0}}(x_{c0}) \mathrm{d}x_{c0},$$

where

$$\mathbb{P}\left[\mathcal{A}_{\mathtt{0,CC}} = 1 | x_{c0}\right] = \sum_{n=1}^{B_C} \mathbb{P}\left[N_{C0} = n | x_{c0}\right] + \sum_{n>B_C} \frac{B_C}{n} \mathbb{P}\left[N_{C0} = n | x_{c0}\right] \quad (29)$$

is the probability that CC user of interest is assigned a pilot in the 0-th cell. Further, conditioned on the event that the 0-th cell has a CE region, the probability of CE user of interest is assigned the l-th pilot is given as

$$\mathbb{E}\left[\mathcal{A}_{\mathtt{0l,CE}} | \mathcal{E}_3^C\right] = \mathbb{P}\left[\mathcal{A}_{\mathtt{0l,CE}} = 1 | \mathcal{E}_3^C\right] = \frac{\mathbb{P}\left[\mathcal{A}_{\mathtt{0,CE}} = 1 | \mathcal{E}_3^C\right]}{B_E}$$
$$= B_E^{-1} \int_0^{\infty} \mathbb{P}\left[\mathcal{A}_{\mathtt{0,CE}} = 1 | \mathcal{E}_3^C, x_{e0}\right] f_{X_{E0}}(x_{e0} | \mathcal{E}_3^C) \mathrm{d}x_{e0},$$

where

$$\mathbb{P}\left[\mathcal{A}_{\mathtt{0,CE}} = 1 | \mathcal{E}_3^C, x_{e0}\right] = \sum_{n=1}^{B_E} \mathbb{P}\left[N_{E0} = n | \mathcal{E}_3^C, x_{e0}\right] + \sum_{n>B_E} \frac{B_E}{n} \mathbb{P}\left[N_{E0} = n | \mathcal{E}_3^C, x_{e0}\right].$$

Proof: The probability of assigning a pilot to the CC user of interest is given as

$$\mathbb{P}\left[\mathcal{A}_{\mathtt{0,CC}} = 1\right] = \mathbb{P}\left[\cup_{n=1}^{B_C} \{\mathcal{A}_{\mathtt{0n,CC}} = 1\}\right]$$
$$= \sum_{n=1}^{B_C} \mathbb{P}\left[\mathcal{A}_{\mathtt{0n,CC}} = 1\right] = B_C \mathbb{P}\left[\mathcal{A}_{\mathtt{0k,CC}} = 1\right],$$

where the last step follows from the fact that the events $\{\{\mathcal{A}_{\mathtt{0n,CC}} = 1\}, n = 1, \ldots, B_C\}$ are equi-probable. Conditioned on the CC area of the 0-th cell, the distribution of the number of users in this region is given by (3). Hence, the probability that the CC user of interest is assigned a pilot is given by (29). The final result is obtained by de-conditioning w.r.t. CC area of the 0-th cell. The pilot assignment probability for the CE user follows from the similar argument. ■

As discussed in Sec. II, since our analysis is performed for the k-th CC (l-th CE) pilot, the aggregate network interference perceived at the 0-th BS depends on the utilization of the k-th CC (l-th CE) pilot in the interfering cells. In the following Lemma, we present the probability of the usage of the k-th CC (l-th CE) pilot in an interfering cell.

Lemma 6. *The probability that the k-th pilot is used in an interfering cell (say j-th cell) is*

$$\mathbb{E}\left[\mathcal{I}_{\mathtt{CC}}(j,k)\right] = \mathbb{P}\left[\mathcal{I}_{\mathtt{CC}}(j,k) = 1\right]$$
$$= \int_0^{\pi R_c^2} \mathbb{P}\left[\mathcal{I}_{\mathtt{CC}}(j,k) = 1 | x_{cj}\right] f_{X_{Cj}}(x_{cj}) \mathrm{d}x_{cj}, \quad (30)$$

where

$$\mathbb{P}\left[\mathcal{I}_{\texttt{CC}}(j,k)=1|x_{cj}\right]=\sum_{n=1}^{B_C}\frac{n}{B_C}\mathbb{P}\left[N_{Cj}=n|x_{cj}\right]+\sum_{n>B_C}\mathbb{P}\left[N_{Cj}=n|x_{cj}\right]. \tag{31}$$

Similarly, conditioned on the event that the j-th cell has a CE region, the probability that the l-th CE pilot is used in the j-th cell is given as $\mathbb{E}\left[\mathcal{I}_{\texttt{CE}}(j,l)|\mathcal{E}_3^C\right]=$

$$\mathbb{P}\left[\mathcal{I}_{\texttt{CE}}(j,l)=1|\mathcal{E}_3^C\right]=\int_{x_{ej}=0}^{\infty}\mathbb{P}\left[\mathcal{I}_{\texttt{CE}}(j,l)=1|\mathcal{E}_3^C,x_{ej}\right]f_{X_{Ej}}(x_{ej}|\mathcal{E}_3^C)\mathrm{d}x_{ej}, \tag{32}$$

where

$$\mathbb{P}\left[\mathcal{I}_{\texttt{CE}}(j,l)=1\middle|\mathcal{E}_3^C,x_{ej}\right]=\sum_{n=1}^{B_E}\frac{n}{B_E}\mathbb{P}\left[N_{Ej}=n\middle|x_{ej},\mathcal{E}_3^C\right]+\sum_{n>B_E}\mathbb{P}\left[N_{Ej}=n\middle|x_{ej},\mathcal{E}_3^C\right].$$

Proof: For the CC case, first we condition on area of the j-th cell. Now, the probability that the k-th pilot is used on the j-th cell is given by (31). The expression in (30) follows from de-conditioning w.r.t. X_{Cj}. On the similar lines, (32) can be derived. ■

V. SINR Coverage and SE Analysis

In this section, we characterize the statistical properties of the point processes $\Phi_{\texttt{u,k}}^{\texttt{CC}}(\Phi_{\texttt{u,l}}^{\texttt{CE}})$ to obtain the coverage probability and SE of a randomly selected CC (CE) user.

A. SINR coverage analysis of a user assigned to the k-th CC pilot

As discussed in Sec. II, $\Phi_{\texttt{u,k}}^{\texttt{CC}}$ is obtained from $\Phi_{\texttt{u,CC}}$. Therefore, the first step is to understand the properties to $\Phi_{\texttt{u,CC}}$, which is discussed next.

1) Density function of $\Phi_{\texttt{u,CC}}$: Conditioned on the 0-th BS location, $\Phi_{\texttt{u,CC}}$ is isotropic. In addition, since $\Phi_{\texttt{u,CC}}$ is defined excluding the point in $\mathcal{X}_c(\mathbf{o},R_c,\Psi_b)$ from $\Psi_{\texttt{u,CC}}$, it is non-homogeneous. Now, our objective is to characterize $\Phi_{\texttt{u,CC}}$ conditioned on the 0-th BS location $\mathbf{o}$. To achieve this objective, we first determine the PCF $g(r)$ of the points in $\Phi_{\texttt{u,CC}}$ w.r.t. $\mathbf{o}$. Next, using this PCF, we approximate the point process as a non-homogeneous PPP. The approach that we have followed for the statistical characterization of $\Phi_{\texttt{u,CC}}$ is inspred by the work presented in [26], where the interfering users are uniformly distributed within the Voronoi cell of each BS. In contrast, in our case the users are uniformly distributed within the CC region of each cell. Hence, our result is slightly more general, i.e. for a sufficiently large value of κ we arrive at the result presented in [26]. Further, as we will see shortly, the derivation of the PCF is also not straightforward as the geometry of the region that we encounter is a little more complex compared to the Voronoi cells considered in [26]. Note that in this case, the PCF $g_\lambda(r,\kappa)$ is also a function of κ. By definition, $g_\lambda(r,\kappa)$ presents the likelihood of finding a point of $\Phi_{\texttt{u,CC}}$ at a distance r from the 0-th BS in a network with $\lambda_0=\lambda$ and threshold radius $R_c=\kappa/\sqrt{\pi c_2\lambda}$. Further, in this case, the PCF is scale-invariant, i.e. $g_\lambda(r,\kappa)=g_1(r\sqrt{\lambda},\kappa)$. Using the scale invariance property, next, we present the PCF of $\Phi_{\texttt{u,CC}}$ w.r.t. origin for $\lambda_0=1$.

Lemma 7. *The PCF of $\Phi_{\texttt{u,CC}}$ w.r.t. the 0-th BS location is*

$$g_1^{\texttt{CC}}(r,\kappa)\approx 1-e^{-2\pi r^2\mathbb{E}\left[X_{C0}(1,\kappa/\sqrt{\pi c_2})^{-1}\right]}, \tag{33}$$

where $X_{C0}(1,\kappa/\sqrt{\pi c_2})$ is the CC area of a typical cell of a PV tessellation with unity BS density.

Proof: Please refer to Appendix B. ■

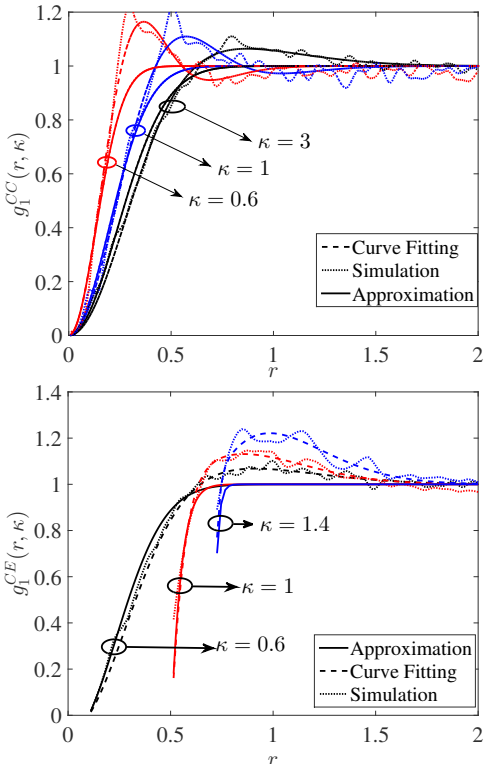

Fig. 3: PCFs of $\Phi_{\texttt{u,CC}}$ (top) and $\Phi_{\texttt{u,CE}}$ (bottom) for different κ. The approximation and curve-fitting are based on (38) and (39), respectively.

In Fig. 3, we present the PCF $g_1^{\texttt{CC}}(r,\kappa)$ for different values of κ. The approximate theoretical expression presented in (33) is compared with the simulation results. Further, following prototype function is also used to approximate the PCF for comparison purpose

$$\hat{g}_1^{\texttt{CC}}(r,\kappa)=1-\exp(-ar^2)+br^2\exp(-cr^2), \tag{34}$$

where the values of the parameters a,b,c are obtained through curve fitting with simulated PCF. Based on the figure, we make the following remark on the PCF in (33).

Remark 2. *For smaller values of κ, the PCF obtained from simulation indicates that $\Phi_{\texttt{u,CC}}$ exhibits clustering behaviour. However, by approximating the PCF using the exponential function presented in* (33)*, it is not possible to capture this*

clustering nature. More complicated functions such as (34) *can be used for this purpose. However, determining the values of the parameters a, b, and c analytically is not tractable. Hence, we resort to the exponential PCF for the rest of the analysis, which is accurate for smaller values of r, i.e. in the neighborhood of the BS at* $\mathbf{o}$.

Using the PCF in (33), we approximate $\Phi_{\mathtt{u},\mathtt{CC}}$ as a non-homogeneous PPP such that for all $f : \mathbb{R}^2 \mapsto \mathbb{R}^+$, $\mathbb{E}\left[\sum_{x\in\Phi_{\mathtt{u},\mathtt{CC}}} f(x)\right] \equiv \mathbb{E}\left[\sum_{x\in\Phi^{\mathrm{PPP}}_{\mathtt{u},\mathtt{CC}}} f(x)\right] \implies$

$$\lambda_0 \int_{\mathbf{x}\in\mathbb{R}^2} f(\mathbf{x}) g_1^{\mathrm{CC}}(\|\mathbf{x}\|\sqrt{\lambda_0},\kappa)\mathrm{d}\mathbf{x} = \int_{\mathbf{x}\in\mathbb{R}^2} f(\mathbf{x})\lambda^{\mathrm{PPP}}_{\mathtt{u},\mathtt{CC}}(\|\mathbf{x}\|,\kappa)\mathrm{d}\mathbf{x},$$

where the second step follows from the application of Campbell's theorem and replacing the intensity measure by the reduced second factorial moment measure [27, Chapter 8]. Hence, the density function of $\Phi_{\mathtt{u},\mathtt{CC}}$, if approximated as a non-homogeneous PPP, is given as

$$\lambda^{\mathrm{PPP}}_{\mathtt{u},\mathtt{CC}}(r,\kappa) = \lambda_0\left(1 - e^{-2\pi\lambda_0 r^2 \mathbb{E}\left[X_{C0}(1,\kappa/\sqrt{\pi c_2})^{-1}\right]}\right). \quad (35)$$

2) Density function of $\Phi^{\mathtt{CC}}_{\mathtt{u},\mathtt{k}}$: Since $\Phi^{\mathtt{CC}}_{\mathtt{u},\mathtt{k}} \subseteq \Phi_{\mathtt{u},\mathtt{CC}}$, one can obtain $\Phi^{\mathtt{CC}}_{\mathtt{u},\mathtt{k}}$ by independently thinning the points in $\Phi_{\mathtt{u},\mathtt{CC}}$ with probability $1 - \mathbb{E}\left[\mathcal{I}_{\mathtt{CC}}(j,k)\right]$. Note that due to correlation in CC areas of neighbouring cells, the number of users in each cell, as well as the pilot utilization probability among neighbouring cells are correlated. Hence, the independent thinning is an approximation. However, to maintain tractability, this approximation is necessary. Approximating $\Phi^{\mathtt{CC}}_{\mathtt{u},\mathtt{k}}$ as a PPP, in the following Lemma, we present its density function.

Lemma 8. *The density function of $\Phi^{\mathtt{CC}}_{\mathtt{u},\mathtt{k}}$ is $\lambda^{\mathtt{CC}}_{\mathtt{u},\mathtt{k}}(r,\kappa) = \lambda_0\mathbb{E}\left[\mathcal{I}_{\mathtt{CC}}(j,k)\right]\left(1 - e^{-2\pi\lambda_0 r^2\mathbb{E}\left[X_{C0}(1,\frac{\kappa}{\sqrt{\pi c_2}})^{-1}\right]}\right)$, where $\mathbb{E}\left[\mathcal{I}_{\mathtt{CC}}(j,k)\right]$ is given in Lemma 6. The intensity measure is $\Lambda^{\mathtt{CC}}_{\mathtt{u},\mathtt{k}}(r,\kappa) = 2\pi\int_0^r \lambda^{\mathtt{CC}}_{\mathtt{u},\mathtt{k}}(t,\kappa)t\mathrm{d}t$.*

Proof: By independently thinning $\Phi^{\mathrm{PPP}}_{\mathtt{u},\mathtt{CC}}$ with probability $1 - \mathbb{E}\left[\mathcal{I}_{\mathtt{CC}}(j,k)\right]$, we arrive at the expression for the density function. ∎

Remark 3. *In the above expression, for $\kappa \to \infty$, $\mathbb{E}\left[X_{C0}(1,\kappa/\sqrt{\pi c_2})^{-1}\right] \approx 7/5$. This corresponds to the interfering user density $\lambda^{\mathrm{PPP}}_{\mathtt{u},\mathtt{CC}}(r,\kappa) \approx \lambda_0\left(1 - \exp\left(-\frac{14}{5}\pi\lambda_0 r^2\right)\right)$, which is the density function for interfering users in case of pilot reuse-1 [26].*
Moreover, since $\lim_{\kappa\to\infty}\mathbb{E}\left[X_{C0}(1,\frac{\kappa}{\sqrt{\pi c_2}})^{-1}\right] \leq \mathbb{E}\left[X_{C0}(1,\frac{\kappa}{\sqrt{\pi c_2}})^{-1}\right]$, the intensity measure of the user point process of pilot reuse-1 is less than $\Lambda^{\mathtt{CC}}_{\mathtt{u},\mathtt{k}}(r,\kappa)$. As a consequence, the distance of the nearest interfering user in case of FPR is stochastically dominated by pilot reuse-1 for a randomly selected CC user.

3) Coverage probability of the CC user of interest: In stochastic geometry-based works, for coverage analysis, one key intermediate step is to characterize the interference by the Laplace transform (LT) of its distribution [14]. The main advantage of this approach is that in the presence of exponential fading gain, the coverage probability can be readily expressed in terms of this LT [14]. However, in the SINR expression given in (10), the small scale fading term is absent due to spatial averaging. Hence, the conventional LT based approach is not applicable in this scenario. Although classical approaches such as Gil-Palaez inversion theorem [35], [36] can be used to obtain coverage probability, it is computationally inefficient, hence, usually avoided wherever possible. A more useful solution to this problem can be obtained by observing the fact that due to pathloss the total interference is likely to be dominated by interference contributions from a few *dominant* users [37]. Based on this intuition, we approximate the total interference power as the sum of the interference power from the *most* dominant interferer and the mean of the rest of the terms conditioned on the dominant term.

Dominant interferer approximation: Let $\hat{D}_{01_k}$ be the distance between the 0-th BS and its nearest interferer. Then, the CDF and the PDF of $\hat{D}_{01_k}$ are given as

$$F_{\hat{D}_{01_k}}(\hat{d}_{01_k}|\kappa) = 1 - e^{-\Lambda^{\mathtt{CC}}_{\mathtt{u},\mathtt{k}}(\hat{d}_{01_k},\kappa)},$$
$$f_{\hat{D}_{01_k}}(\hat{d}_{01_k}|\kappa) = 2\pi\hat{d}_{01_k}\lambda^{\mathtt{CC}}_{\mathtt{u},\mathtt{k}}(\hat{d}_{01_k},\kappa)e^{-\Lambda^{\mathtt{CC}}_{\mathtt{u},\mathtt{k}}(\hat{d}_{01_k},\kappa)}, \quad (36)$$

which are obtained using void probability of the PPP [14]. Now, the total interference is approximated as the sum of interference from the most dominant interferer and the expected interference from rest of the interferers in the network. Hence, we write $I_{\mathtt{agg},k} = \hat{D}^{-2\alpha}_{01_k} + \mathbb{E}\left[\sum_{\hat{\mathbf{u}}_{j_k}\in\Phi^{\mathtt{CC}}_{\mathtt{u},\mathtt{k}}\setminus\hat{\mathbf{u}}_{1_k}} \hat{D}^{-2\alpha}_{0j_k}\middle|\hat{D}_{01_k}\right] = \hat{D}^{-2\alpha}_{01_k} + \mathbb{E}\left[I_{\mathtt{rem},\mathtt{k}}|\hat{D}_{01_k}\right]$, where $\hat{\mathbf{u}}_{1_k}$ is the location of the dominant interferer in $\Phi^{\mathtt{CC}}_{\mathtt{u},\mathtt{k}}$. In the following Lemma, we present an expression for $\mathbb{E}\left[I_{\mathtt{rem},\mathtt{k}}|\hat{D}_{01_k}\right]$.

Lemma 9. *Conditioned on the distance to the dominant interferer $\hat{D}_{01_k}$, the expected interference from the rest of the interfering users is $\mathbb{E}\left[I_{\mathtt{rem},\mathtt{k}}|\hat{D}_{01_k} = \hat{d}_{01_k}\right] = 2\pi\int_{\hat{d}_{01_k}}^{\infty} r^{-2\alpha}\lambda^{\mathtt{CC}}_{\mathtt{u},\mathtt{k}}(r,\kappa)r\mathrm{d}r$.*

Proof: Above expression follows from the application of Campbell's theorem. ∎

With the knowledge of the expected interference and the distribution of $\hat{D}_{01_k}$, in the following proposition, we present the coverage probability for a CC user assigned to the k-th pilot.

Proposition 1. *Conditioned on the event that the k-th pilot is used in the 0-th cell, the coverage probability of the user that is assigned this sequence is given as $\mathtt{P}^{\mathtt{CC}}_{\mathtt{c},\mathtt{k}}(T) =$*

$$\mathbb{E}_{D_{00_k},\hat{D}_{01_k}}\left[\mathbf{1}\left(\hat{d}^{-2\alpha}_{01_k} + \mathbb{E}\left[I_{\mathtt{rem},\mathtt{k}}|\hat{d}_{01_k}\right] < \frac{d^{-2\alpha}_{00_k}}{T}\right)\middle|\mathcal{I}_{\mathtt{CC}}(0,k) = 1\right], \quad (37)$$

where $f_{\hat{D}_{01_k}}(\hat{d}_{01_k})$ is given in (36)*, and the CDF of D_{00_k} is given in* (6)*.*

Proof: Conditioned on $\mathcal{I}_{\mathtt{CC}}(0,k) = 1$, the coverage probability of the user assigned the k-th sequence is

$$\mathbb{P}\left[\mathtt{SINR}_{0_k} > T | \mathcal{I}_{\mathtt{CC}}(0,k)=1\right] =$$
$$\mathbb{P}\left[\frac{D_{00_k}^{-2\alpha}}{T} > I_{\mathtt{agg,k}} \middle| \mathcal{I}_{\mathtt{CC}}(0,k)=1\right]$$
$$=\mathbb{E}\left[\mathbf{1}\left(\hat{d}_{01_k}^{-2\alpha} + \mathbb{E}\left[I_{\mathtt{rem,k}}|\hat{d}_{01_k}\right] < \frac{d_{00_k}^{-2\alpha}}{T}\right)\middle| \mathcal{I}_{\mathtt{CC}}(0,k)=1\right],$$

where the expectation is taken over $D_{00_k}, \hat{D}_{01_k}$. This completes the proof of the above proposition. ∎

B. SINR *coverage analysis of a CE user assigned to the l-th CE pilot*

Most of the intermediate steps necessary for the coverage probability result in this case can be derived on the similar lines as that of the previous section. Hence, we omit a few of the proofs to avoid repetition.

1) Density function of $\Phi_{\mathtt{u,l}}^{\mathtt{CE}}$: To begin with, we present the density function of the point process $\Phi_{\mathtt{u,CE}}$. Similar to the CC case, we first present the PCF $g_{\lambda}^{\mathrm{CE}}(r,\kappa)$ for $\Phi_{\mathtt{u,CE}}$ w.r.t. the 0-th BS. Due to scale invariance, we consider a network with unit BS density and threshold radius $\kappa/\sqrt{\pi c_2}$. In the following Lemma, we present the expression for $g_1^{\mathrm{CE}}(r,\kappa)$.

Lemma 10. *The PCF of $\Phi_{\mathtt{u,CE}}$ w.r.t. the 0-th BS is given as*

$$g_1^{\mathrm{CE}}(r,\kappa) \approx 1 - e^{-\pi\left(r^2 - \frac{\kappa^2}{\pi c_2}\right)\frac{14}{5}\mathbb{P}\left[\mathcal{E}_3^C\right]\exp(\kappa^2/c_2)}, \quad r \geq \frac{\kappa}{\sqrt{\pi c_2}}. \tag{38}$$

Proof: Please refer to Appendix D. ∎

Similar to the CC case, in Fig. 3, we present the PCF for different values of κ for $\Phi_{\mathtt{u,CE}}$. The approximate theoretical expression presented in (38) is compared with the simulation results. We use the following prototype function to approximate the PCF for comparison purpose

$$\hat{g}_1^{\mathrm{CE}}(r,\kappa) = 1 - e^{-a_1(r^2-R_c^2)} + b_1(r^2-R_c^2)e^{-c_1(r^2-R_c^2)}, \tag{39}$$

where the values of the parameters a_1, b_1, c_1 are obtained through curve fitting with simulated PCF. Based on the figure, we make the following remark for the PCF in (38).

Remark 4. *As κ increases, the PCF obtained from simulation indicates that $\Phi_{\mathtt{u,CE}}$ exhibits clustering behaviour beyond R_c. By approximating the PCF using the exponential function presented in* (38)*, it is not possible to capture this clustering nature. However, note that from the network deployment perspective higher values of R_c may not be desirable, because it would result in a higher fraction of cells without CE regions. Hence, the benefit of FPR will be reduced due to unutilized CE pilots in the cells without the CE regions. Therefore, the range of κ for which the approximation of PCF using* (38) *is poor is of lesser practical importance.*

Now, we approximate $\Phi_{\mathtt{u,CE}}$ as a non-homogeneous PPP with density function $\lambda_{\mathtt{u,CE}}^{\mathrm{PPP}}(r,\kappa) =$

$$\lambda_0 \mathbb{P}\left[\mathcal{E}_3^C\right]\left(1 - e^{-\pi\lambda_0(r^2-R_c^2)\mathbb{P}\left[\mathcal{E}_3^C\right]\frac{14}{5}\exp(\kappa^2/c_2)}\right), \quad r \geq R_c. \tag{40}$$

Recall that $\Phi_{\mathtt{u,l}}^{\mathtt{CE}} \subseteq \Phi_{\mathtt{u,CE}}$ contains the locations of the interfering CE users that use the l-th pilot. Similar to the CC case, we approximate $\Phi_{\mathtt{u,l}}^{\mathtt{CE}}$ as a non-homogeneous PPP whose density function is presented in the following lemma.

Lemma 11. *For $r \geq R_c$, the density function of the $\Phi_{\mathtt{u,l}}^{\mathtt{CE}}$ containing the locations of the active CE interfering users is approximated as $\lambda_{\mathtt{u,l}}^{\mathtt{CE}}(r,\kappa) \approx \lambda_0 \mathbb{E}\left[\mathcal{I}_{\mathtt{CE}}(j,l)\right]\mathbb{P}\left[\mathcal{E}_3^C\right]\left(1 - e^{-\pi\frac{14}{5}\exp(\kappa^2/c_2)\mathbb{P}\left[\mathcal{E}_3^C\right]\lambda_0(r^2-R_c^2)}\right)$, and corresponding intensity measure is given as $\Lambda_{\mathtt{u,l}}^{\mathtt{CE}}(r,\kappa) = 2\pi\int_{t=0}^{r}\lambda_{\mathtt{u,l}}^{\mathtt{CE}}(t,\kappa)t\mathrm{d}t$.*

Proof: The density function is obtained on the similar arguments as that of Lemma 8. ∎

2) Coverage probability of the CE user of interest: Using the intensity measure and density function of $\Phi_{\mathtt{u,l}}^{\mathtt{CE}}$, the CDF and PDF of the distance to the dominant CE interferer are given as

$$F_{\hat{D}_{01_l}}(\hat{d}_{01_l}|\kappa) = 1 - e^{-\Lambda_{\mathtt{u,l}}^{\mathtt{CE}}(\hat{d}_{01_l},\kappa)}, \tag{41}$$
$$f_{\hat{D}_{01_l}}(\hat{d}_{01_l}|\kappa) = 2\pi\hat{d}_{01_l}\lambda_{\mathtt{u,l}}^{\mathtt{CE}}(\hat{d}_{01_l},\kappa)e^{-\Lambda_{\mathtt{u,l}}^{\mathtt{CE}}(\hat{d}_{01_l},\kappa)}. \tag{42}$$

Now, conditioned on the distance to the dominant interferer $\hat{D}_{01_l}$, the aggregate interference at the 0-th BS from the CE users is approximated as

$$I_{\mathtt{agg,l}} = \hat{d}_{01_l}^{-2\alpha} + \mathbb{E}\left[\sum_{\hat{\mathbf{u}}_{j_l}\in\Phi_{\mathtt{u,l}}^{\mathtt{CE}}\setminus\hat{\mathbf{u}}_{1_l}} \hat{d}_{0j_l}^{-2\alpha}\middle|\hat{d}_{01_l}\right]$$
$$= \hat{d}_{01_l}^{-2\alpha} + \mathbb{E}\left[I_{\mathtt{rem,l}}\middle|\hat{d}_{01_l}\right]$$
$$\overset{(a)}{=} \hat{d}_{01_l}^{-2\alpha} + 2\pi\int_{\hat{d}_{01_l}}^{\infty} r^{-2\alpha}\lambda_{\mathtt{u,l}}^{\mathtt{CE}}(r,\kappa)r\mathrm{d}r,$$

where (a) follows from the application of Campbell's theorem. Using the above expression for aggregate interference, the coverage probability of the CE user of interest is presented next.

Proposition 2. *Conditioned on the event that $\mathcal{I}_{\mathtt{CE}}(0,l)=1$, the coverage probability of a user assigned to l-th pilot is given as $\mathtt{P}_{\mathtt{c,l}}^{\mathtt{CE}}(T) = \mathbb{P}\left[\mathtt{SINR}_{0,1} > T|\mathcal{E}_3^C, \mathcal{I}_{\mathtt{CE}}(0,l)=1\right] =$*

$$\mathbb{E}_{D_{00_l},\hat{D}_{01_l}}\left[\mathbf{1}\left(I_{\mathtt{agg,l}} < \frac{d_{00_l}^{-2\alpha}}{T}\right)\middle|\mathcal{E}_3^C, \mathcal{I}_{\mathtt{CE}}(0,l)=1\right].$$

Proof: The proof can be done on the similar lines as that of Proposition 1. ∎

C. Average user SE and cell SE

Using the coverage probability results, in the following Proposition, we present the approximate expressions for average SE of the CC and CE users of interest, and average cell SE. It is worthwhile mentioning that alternate methods such as the one presented in [38], [39] can also be used to characterize the SE.

Proposition 3. *The average SE of a randomly selected CC user is given as*

$$\overline{\mathtt{SE}}_{\mathtt{u,CC}} \approx \omega B_C \mathbb{E}\left[\mathcal{A}_{\mathtt{0k,CC}}\right]\int_{t=0}^{\infty}\mathtt{P}_{\mathtt{c,k}}^{\mathtt{CC}}(2^t-1)\mathrm{d}t, \tag{43}$$

where $\omega = (1 - B/T_C)$, $\mathtt{P}^{\mathtt{CC}}_{\mathtt{c},\mathtt{k}}(\cdot)$ *is presented in Proposition 1 and* $\mathbb{E}\left[\mathcal{A}_{\mathtt{0k},\mathtt{CC}}\right]$ *is presented in Lemma 5. Similarly, the average SE of a randomly selected CE user is given as*

$$\overline{\mathtt{SE}}_{\mathtt{u},\mathtt{CE}} \approx \omega B_E \mathbb{E}\left[\mathcal{A}_{\mathtt{0l},\mathtt{CE}} | \mathcal{E}_3^C\right] \int_{t=0}^{\infty} \mathtt{P}^{\mathtt{CE}}_{\mathtt{c},\mathtt{l}}(2^t - 1)\mathrm{d}t. \tag{44}$$

Proof: From (11), the average SE of the CC user of interest can be approximated as

$$\begin{aligned}
\overline{\mathtt{SE}}_{\mathtt{u},\mathtt{CC}} =& \omega \mathbb{E}\left[\mathcal{A}_{\mathtt{0},\mathtt{CC}} \log_2(1 + \mathtt{SINR}_{\mathtt{0},\mathtt{CC}})\right] \\
=& \omega \mathbb{E}\left[\sum_{n=1}^{B_C} \mathcal{A}_{\mathtt{0n},\mathtt{CC}} \log_2(1 + \mathtt{SINR}_{0_n})\right] \\
\overset{(a)}{=}& B_C \mathbb{E}\left[\mathcal{A}_{\mathtt{0k},\mathtt{CC}} \log_2(1 + \mathtt{SINR}_{0_k})\right] \\
\overset{(b)}{\approx}& B_C \mathbb{E}\left[\mathcal{A}_{\mathtt{0k},\mathtt{CC}}\right] \mathbb{E}\left[\log_2(1 + \mathtt{SINR}_{0_k})\right],
\end{aligned}$$

where $\mathtt{SINR}_{0_n}$ is the $\mathtt{SINR}$ of the CC user of interest if it is assigned the n-th CC pilot, (a) follows from the identical distributions of $\{\mathcal{A}_{\mathtt{0n},\mathtt{CC}} \log_2(1 + \mathtt{SINR}_{0_n})\}_{n=1}^{B_C}$, (b) follows from the independence assumption between $\mathcal{A}_{\mathtt{0k},\mathtt{CC}}$ and $\mathtt{SINR}_{0_k}$. The expression in the proposition follows from the last step using the fact that for a positive random variable X, $\mathbb{E}[X] = \int_0^\infty \mathbb{P}[X > t]\,\mathrm{d}t$. Similarly, the average CE user SE is derived. ∎

Proposition 4. *The average cell SE of a typical cell is given as*

$$\begin{aligned}
\overline{\mathtt{CSE}} =& \omega B_C \mathbb{E}\left[\mathcal{I}_{\mathtt{CC}}(0,k)\right] \int_{t=0}^{\infty} \mathtt{P}^{\mathtt{CC}}_{\mathtt{c},\mathtt{k}}(2^t - 1)\mathrm{d}t \\
&+ \omega \mathbb{P}\left[\mathcal{E}_3^C\right] B_E \mathbb{E}\left[\mathcal{I}_{\mathtt{CE}}(0,l) | \mathcal{E}_3^C\right] \int_{t=0}^{\infty} \mathtt{P}^{\mathtt{CE}}_{\mathtt{c},\mathtt{l}}(2^t - 1)\mathrm{d}t.
\end{aligned}$$

Proof: From (12), we write

$$\begin{aligned}
\mathbb{E}\left[\mathtt{CSE}\right] \overset{(a)}{=}& \omega \mathbb{E}\left[\sum_{n=1}^{B_C} \mathcal{I}_{\mathtt{CC}}(0,n) \log_2(1 + \mathtt{SINR}_{0_n})\right] + \\
& \omega \mathbb{P}\left[\mathcal{E}_3^C\right] \mathbb{E}\left[\sum_{m=1}^{B_E} \mathcal{I}_{\mathtt{CE}}(0,m) \log_2(1 + \mathtt{SINR}_{0_m}) \middle| \mathcal{E}_3^C\right] \\
\overset{(b)}{\approx}& \omega B_C \mathbb{E}\left[\log_2(1 + \mathtt{SINR}_{0_k}) | \mathcal{I}_{\mathtt{CC}}(0,k) = 1\right] \times \\
& \mathbb{E}\left[\mathcal{I}_{\mathtt{CC}}(0,k)\right] + \omega B_E \mathbb{P}\left[\mathcal{E}_3^C\right] \mathbb{E}\left[\mathcal{I}_{\mathtt{CE}}(0,l) | \mathcal{E}_3^C\right] \times \\
& \mathbb{E}\left[\log_2(1 + \mathtt{SINR}_{0_l}) | \mathcal{I}_{\mathtt{CE}}(0,l) = 1, \mathcal{E}_3^C\right],
\end{aligned}$$

where (a) follows from the law of total probability and (b) follows from the fact that $\{\mathtt{SINR}_{0_n}\}_{n=1}^{B_C}$ ($\{\mathtt{SINR}_{0_m}\}_{m=1}^{B_E}$) are identical, and for the final expression we assume independence between the event $\{\mathcal{I}_{\mathtt{CC}}(0,k) = 1\}$ and $\mathtt{SINR}_{0_k}$ and use the identity $\mathbb{E}[X] = \int_0^\infty \mathbb{P}[X > t]\,\mathrm{d}t$. ∎

VI. Numerical Results and Discussion

In this section, we validate the approximate theoretical results using Monte Carlo simulations. Further, we study the effect of different system parameters on the $\mathtt{SINR}$ coverage probability, average user and cell SEs. In our simulation framework, we consider the BS density $\lambda_0 = 4 \times 10^{-6}$, pathloss exponent $\alpha = 3.7$, the coherence time interval $T_c = 200$ symbol duration, and the pilot length $B = 100$ symbol duration. For comparison purpose, we also provide SE results corresponding to pilot reuse-1 at necessary places. Note that the system model for reuse-1 is the same as described in Sec. II. The key difference is that there is no segregation in terms of CC (CE) pilots and the entire set of B pilots can be assigned to any user attached to a BS. This complicates the pilot utilization analysis. To be specific, to obtain the probability of the event that a CC (CE) user is assigned a given pilot requires the consideration of the joint distribution of the number of CC and CE users. This result does not directly follow from Lemma 5 and requires additional analysis, which does not appear tractable as deriving joint distribution for the CC and CE areas of a typical cell is challenging. The similar remark holds for the probability of pilot utilization in case of reuse-1. Hence, to validate the efficacy of FPR scheme with respect to reuse-1, we rely on simulation-based results for reuse-1.

A. $\mathtt{SINR}$ coverage probability of a user assigned to a given pilot

In this subsection, we study the effect of different system parameters on the coverage probability of a CC (CE) user that is assigned the k-th (l-th) pilot. The effect of λ_u on coverage probability for CC and CE cases can be observed from Fig. 4 (left and right, respectively). From the figures, we infer that with the increasing density, the coverage probability reduces in both the scenarios. This is intuitive as with increasing λ_u, the pilot usage probability in the interfering cells increases, thereby increasing the aggregate interference. The effect of normalized threshold radius κ on coverage probability is presented in Fig. 5 for CC (left) and CE (right) cases. As observed from Fig. 5 (left), with decreasing κ (equivalently R_c), the coverage probability improves. This behavior is justified by the fact that with decreasing R_c the serving distance also decreases. In addition, the pilot usage probability in interfering cells also reduces. Combination of both the effects results in $\mathtt{SINR}$ coverage probability improvement. For a randomly selected CE user assigned a given CE pilot sequence, above trend is observed for higher $\mathtt{SINR}$ thresholds. On the other hand, for lower $\mathtt{SINR}$ thresholds, reverse trend is observed. One possible explanation behind this behaviour is that although with increasing R_c serving distance increases, the number of interfering users reduces. This results in improvement of coverage probability. In Fig. 6, we have presented coverage probability for different path loss exponent α. As expected with increasing path loss exponent, the coverage probability improves due to less interference.

B. Average CC (CE) user SE and cell SE

SE as a function of B_C/B: In Fig. 7, the average SEs of CC and CE users of interest as well as a typical cell are presented for different values of B_C/B, where $B = 100$. For reference, we have also presented the average CC and CE user SEs for unity pilot reuse. From Fig. 7 (left), we observe that FPR scheme performs better compared to unity reuse beyond a certain B_C/B. For both the curves (corresponding to $\kappa = 0.8, 1$), this value of B_C/B lies in the neighbourhood of $1 -$

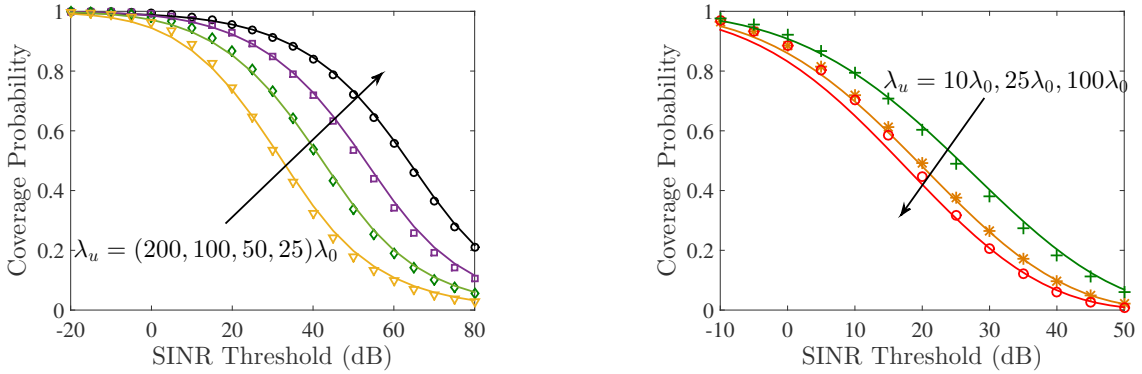

Fig. 4: Coverage probability of a CC user on a given CC pilot (left) and CE user on a given CE pilot (right) for different λ_u. Markers and solid lines represent the simulation and theoretical results, respectively. $\kappa = 0.6, B_C = 58, B_E = 14, \beta_f = 3$.

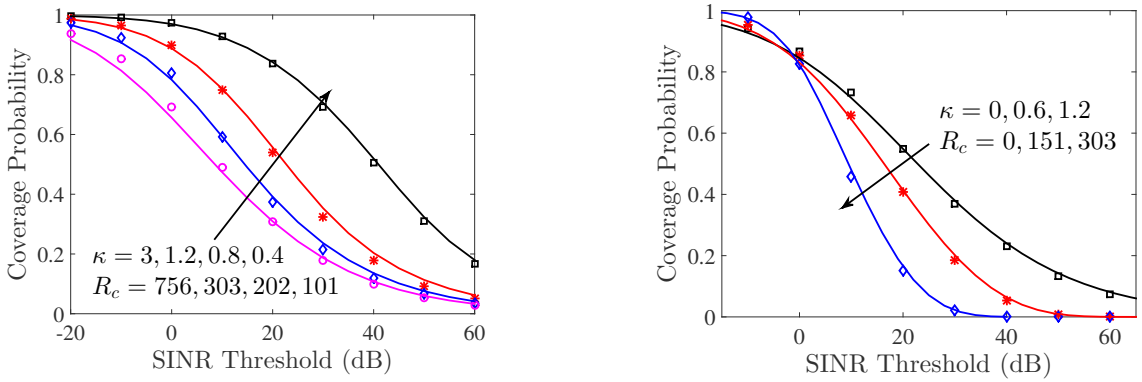

Fig. 5: Coverage probability of a CC user on a given CC pilot (left) and CE user on a given CE pilot (right) for different R_c. Markers and solid lines represent the simulation and theoretical results, respectively. $B_C = 58, B_E = 14, \beta_f = 3, \mathbb{E}\left[\mathcal{I}_{\text{CC}}(0,k)\right] = \mathbb{E}\left[\mathcal{I}_{\text{CE}}(0,l)|\mathcal{E}_3^C\right] = 1$.

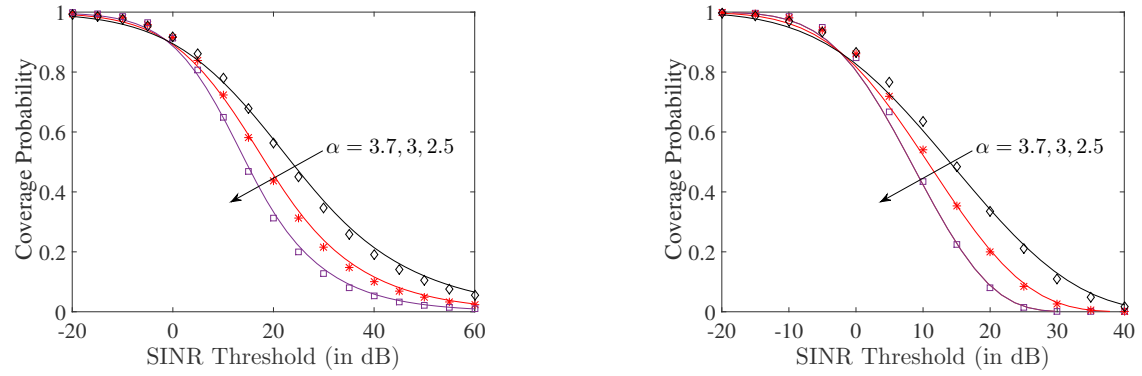

Fig. 6: Coverage probability of a CC user on a given CC pilot (left) and CE user on a given CE pilot (right) for different path loss exponent α. Markers and solid lines represent the simulation and theoretical results, respectively. $\kappa = 0.8, B_C = 49, B_E = 17, \beta_f = 3$.

$\exp(-\kappa^2)$. Intuitively, in case of unity reuse, the probability of assigning a pilot sequence to a CC user is approximately $1 - \exp(-\pi\lambda_0 c_2 R_c^2) = 1 - \exp(-\kappa^2)$. Hence, on an average $1 - \exp(-\kappa^2)$ fraction of pilot sequences are assigned to CC users. Therefore, by choosing $B_C/B \approx 1 - \exp(-\kappa^2)$ in FPR case, the average SE for CC user of interest becomes close to the SE of a CC user in unity reuse. On the other hand, from Fig. 7 (middle), we observe that for a wide-range of B_C/B the average SE of CE user of interest in FPR is higher compared to average CE user SE in case of unity reuse. This result justifies the use of FPR scheme as its main purpose is to improve the performance of CE users. Finally, the average cell SE for FPR scheme is presented in Fig. 7 (right) for two different values of κ. For comparison purpose, the cell SEs corresponding to reuse-1 is also presented. Depending on the value of κ, for certain values of B_C/B, sum-cell SE gains over reuse-1 is possible.

SE as a function of κ: The average SEs for the three cases of interest (CC user of interest, CE user of interest, and sum-cell) are presented in Fig. 8 for different values of κ. Based on the insights from the previous result, in order to achieve the same CC user SE as reuse-1, we partition the pilot sequences into two sets such that $B_C/B \approx 1 - \exp(-\kappa^2)$.

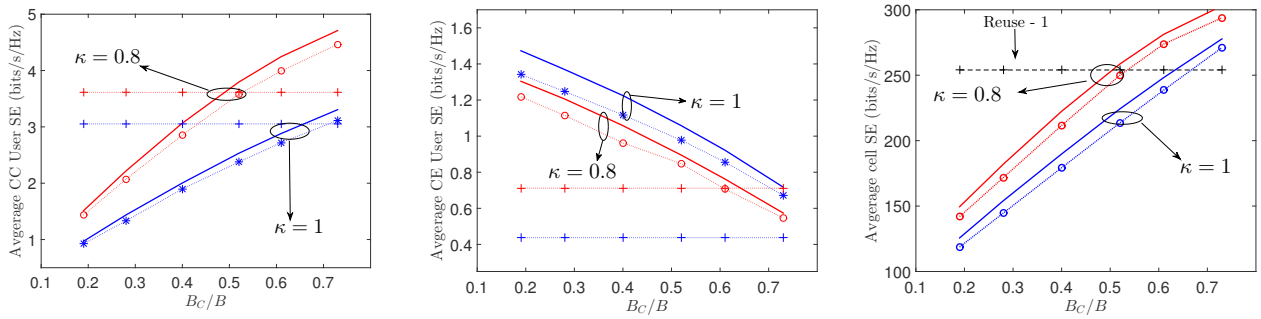

Fig. 7: The average CC user SE (left), CE user SE (center), and sum-cell SE (right) as functions of B_C/B. The solid lines and marked dotted lines represent the theoretical and simulation results, respectively. The dashed lines represent the simulated SEs corresponding to reuse-1. $B = 100, \lambda_u = 150\lambda_0, \lambda_0 = 4 \times 10^{-6}, \beta_f = 3$.

From Fig. 8 (left), we observe that aforementioned partitioning rule results in marginal reduction in CC user SE compared to reuse-1 scheme. On the other hand, in Fig. 8 (middle), we observe that the CE user spectral efficiency of reuse-1 is better compared to the FPR scheme for lower values of κ. This is because of the fact that when κ is low, more number of users lie in the CE region. Since FPR employs reuse-3 scheme, the pilot assignment probability to a randomly selected user reduces, which results in the reduction of user SE compared to the reuse-1 scheme. However, for higher values of κ, FPR performs better compared to the reuse-1 scheme, which is the desired outcome. From Fig. 8 (right), we observe that the average sum-cell SE in case of FPR scheme is close to reuse-1 scheme for higher values of κ with the above partitioning rule. System operation at this point is desirable as it improves the CE user SE while providing comparable CC user SE.

SE as a function of B/T_c: From Fig. 9, we observe that average SEs are concave functions of B/T_c. Note that with increasing B/T_c, the pilot assignment probability increases and the SINR improves due to reduced pilot utilization in the interfering cells. On the other hand, the pre-log factor $(1-B/T_c)$ reduces with increasing B/T_c. Hence, the concave behavior of the functions is justified. Further, we observe that using the proposed pilot partitioning rule, there is a significant improvement in the CE user SE at the cost of marginal reductions in average CC user SE and average sum-cell SE.

In Fig. 10, we show he effect of user density on SE. As expected, with increasing user density, the average user SEs reduces while the sum-cell SE saturates.

VII. Concluding Remarks

In this work, we have analyzed the UL performance of a mMIMO system with fractional pilot reuse. Using tools from stochastic geometry, we have presented approximate expressions for the SINR coverage probability and average SE of a randomly CC (CE) user in a typical cell. Our analysis begins with the accurate approximations of the area distributions of CC and CE regions of a typical cell. These distributions are used to analyze the pilot assignment probability for the user of interest and utilization probability of a given pilot sequence in a typical cell. While the former quantity is directly used in average user SE evaluation, the latter quantity is helpful in obtaining the average sum-cell SE and statistical characterization of interfering user point processes for both CC and CE cases. All the theoretical results are validated through extensive Monte Carlo simulations. From our system analysis, we arrive at the conclusion that with proper selection of system parameters it is possible to improve the CE user SE with negligible performance degradation in the CC user SE and cell SE compared to the unity pilot reuse. There are several possible extensions of this work. In this work, we have considered an asymptotically large number of antennas at the BSs. Hence, a natural extension of this work is to consider a system with finite number of antennas and evaluate the efficacy of FPR. From stochastic geometry perspective, our analysis of interfering user point process formed by CE users can be improved further by modeling this point process as a cluster process or a Poisson hole process [40].

Appendix

A. Proof of Lemma 1

The mean area of the CE region can be expresses as $\mathbb{E}\left[|\mathcal{X}_E(\mathbf{o}, R_c, \Psi_b)|\right] =$

$$\mathbb{E}\left[\int_{\mathbf{x}\in\mathbb{R}^2} \mathbf{1}_{(\mathbf{x}\in\mathcal{V}_{\Psi_b}(\mathbf{o})\cap\mathcal{B}^C_{R_c}(\mathbf{o}))}\mathrm{d}\mathbf{x}\right]$$
$$\overset{(a)}{=}\int_{\mathbf{x}\in\mathbb{R}^2\cap\mathcal{B}^C_{R_c}(\mathbf{o})} \exp(-\pi\lambda_0\|\mathbf{x}\|^2)\mathrm{d}\mathbf{x}$$
$$=2\pi\int_{r=R_c}^{\infty}\exp(-\pi\lambda_0 r^2)r\mathrm{d}r,$$

where (a) follows from that fact that a point located at a distance $\|\mathbf{x}\|$ from the origin belongs to $\mathcal{V}_{\Psi_b}(\mathbf{o})$, if there are no other BSs in $\mathcal{B}_{\|\mathbf{x}\|}(\mathbf{x})$. Solving the final integral gives us the expression for the mean in (21). Similarly, the second moment of the CE area can be expressed as $\mathbb{E}\left[|\mathcal{X}_E(\mathbf{o}, R_c, \Psi_b)|^2\right] =$

$$\mathbb{E}\left[\int_{\mathbf{x}\in\mathbb{R}^2} \mathbf{1}_{(\mathbf{x}\in\mathcal{V}_{\Psi_b}(\mathbf{o})\cap\mathcal{B}^C_{R_c}(\mathbf{o}))}\mathrm{d}\mathbf{x}\int_{\mathbf{y}\in\mathbb{R}^2} \mathbf{1}_{(\mathbf{y}\in\mathcal{V}_{\Psi_b}(\mathbf{o})\cap\mathcal{B}^C_{R_c}(\mathbf{o}))}\mathrm{d}\mathbf{y}\right]$$
$$=\int_{\mathbf{x}\in\mathbb{R}^2}\int_{\mathbf{y}\in\mathbb{R}^2}\mathbb{E}\left[\mathbf{1}_{(\mathbf{x}\in\mathcal{V}_{\Psi_b}(\mathbf{o})\cap\mathcal{B}^C_{R_c}(\mathbf{o}),\mathbf{y}\in\mathcal{V}_{\Psi_b}(\mathbf{o})\cap\mathcal{B}^C_{R_c}(\mathbf{o}))}\right]\mathrm{d}\mathbf{x}\mathrm{d}\mathbf{y}$$

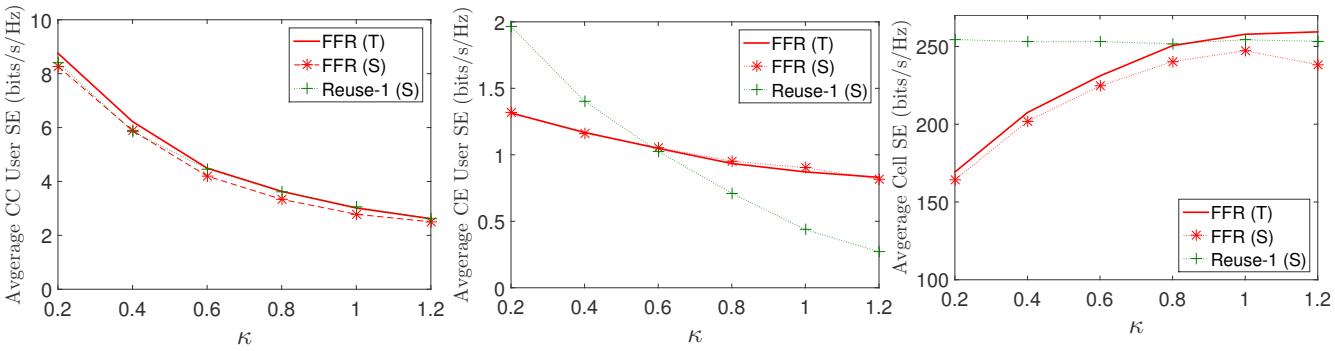

Fig. 8: The average CC user SE (left), CE user SE (center), and sum-cell SE (right) as functions of normalized radius κ. $\lambda_0 = 4 \times 10^{-6}, \lambda_u = 150\lambda_0, B_C/B \approx \left(1 - \exp(-\kappa^2)\right), \beta_f = 3$. The solid lines and marked dotted lines represent the theoretical and simulation results, respectively.

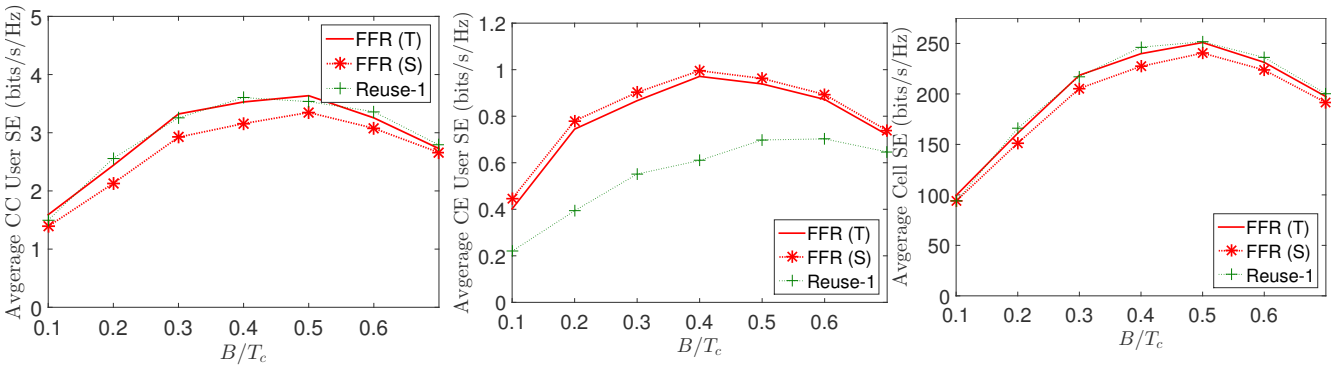

Fig. 9: The average CC user SE (left), CE user SE (center), and sum-cell SE (right) as functions of B/T_c. The solid lines and marked dotted lines represent the theoretical and simulation results, respectively. $\kappa = 0.8, \beta_f = 3, B_C/B \approx \left(1 - \exp(-\kappa^2)\right)$.

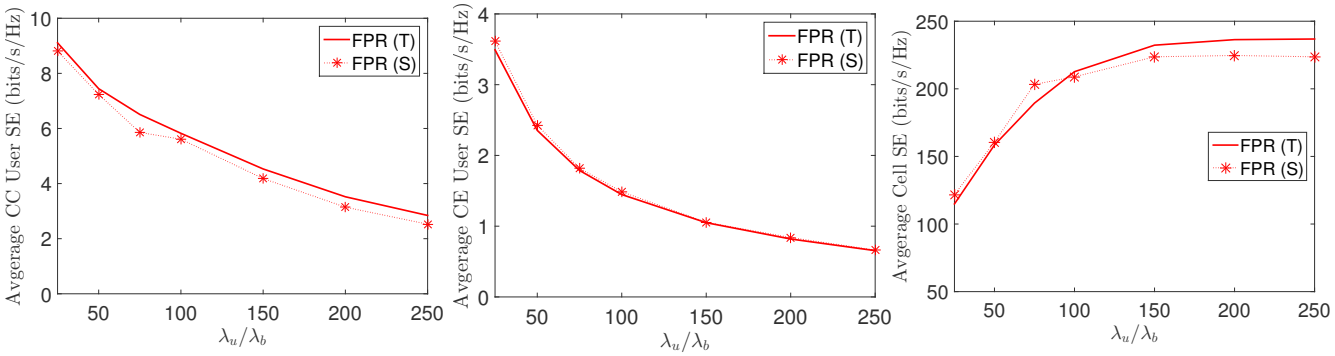

Fig. 10: Average user SE of a randomly selected CC user (left), CE user (center), and average sum-cell SE (right) as a function of λ_u/λ_b. The solid lines and marked dotted lines represent the theoretical and simulation results, respectively. $B = 100, B_C = 31, \kappa = 0.6, \beta_f = 3$.

$$\overset{(b)}{=} \int\limits_{(\mathbf{x},\mathbf{y})\in\mathbb{R}^2\cap\mathcal{B}^C_{R_c}(\mathbf{o})\times\mathbb{R}^2\cap\mathcal{B}^C_{R_c}(\mathbf{o})} e^{-\lambda_0|\mathcal{B}_{\|\mathbf{x}\|}(\mathbf{x})\cup\mathcal{B}_{\|\mathbf{y}\|}(\mathbf{y})|}\mathrm{d}\mathbf{x}\mathrm{d}\mathbf{y}$$

$$= 2\pi \int\limits_{r_1=R_c}^{\infty}\int\limits_{r_2=R_c}^{\infty}\int\limits_{u=0}^{2\pi} e^{-\lambda_0 V(r_1,r_2,u)}\mathrm{d}u r_2\mathrm{d}r_2 r_1\mathrm{d}r_1,$$

where (b) follows from the fact that if points $\mathbf{x}$ and $\mathbf{y}$ belong to $\mathcal{V}_{\Psi_b}(\mathbf{o})$, then there are no other BSs in the region $\mathcal{B}_{\|\mathbf{x}\|}(\mathbf{x}) \cup \mathcal{B}_{\|\mathbf{y}\|}(\mathbf{y})$, and the last step follows from changing the integration limits from Cartesian to polar coordinates. ■

B. Proof of Lemma 7

One approach to deriving $g_1^{\mathrm{CC}}(r,\kappa)$ is to first determine the Ripley's K-function $K_1^{\mathrm{CC}}(r,\kappa)$ and then use the following relationship: $g_1^{\mathrm{CC}}(r,\kappa) = \frac{\mathrm{d}K_1^{\mathrm{CC}}(r,\kappa)/\mathrm{d}r}{2\pi r}$. Note that points in $\Phi_{\mathrm{u,cc}}$ are likely to exhibit repulsion w.r.t. $\mathbf{o}$ as these points do not lie in $\mathcal{V}_{\Psi_b}(\mathbf{o})$. Since the total interference is likely to be dominated by the nearby users, our main interest lies in characterizing $g_1^{\mathrm{CC}}(r,\kappa)$ for small r. Note that $g_1^{\mathrm{CC}}(r,\kappa) \to 1$ as $r \gg 0$. Recall that for a point process Φ of density λ the Ripley's K-function is defined as $K_\lambda(r) = \mathbb{E}\left[N_\Phi(\mathcal{B}_r(\mathbf{o}))\right]/\lambda$ [27], where $N_\Phi(\mathcal{B}_r(\mathbf{o}))$ denotes the number of points of Φ that lie in $\mathcal{B}_r(\mathbf{o})$. In this case, the K-function is given as $K_1^{\mathrm{CC}}(r,\kappa) =$

$\mathbb{E}\left[N_{\Phi_{\mathrm{u,cc}}}\left(\cup_{\mathbf{x}\in\Phi_b}(\mathcal{B}_r(\mathbf{o})\cap\mathcal{X}_C(\mathbf{x},\kappa/\sqrt{\pi c_2},\Psi_b))\right)\right]$. Now,

$$\begin{aligned}&K_1^{\mathrm{CC}}(r,\kappa)\\ \simeq&\mathbb{E}\left[N_{\Phi_{\mathrm{u,cc}}}\left(\mathcal{B}_r(\mathbf{o})\cap\mathcal{X}_C(\mathbf{y},\kappa/\sqrt{\pi c_2},\Psi_b)\right)\right],\quad r\to 0,\end{aligned}\tag{45}$$

where $\simeq$ denotes approximation that becomes better asymptotically, $\mathbf{y}$ is the nearest BS to the typical BS at $\mathbf{o}$. Without loss of generality, we assume that $\mathbf{y}=(\|\mathbf{y}\|,0)$. As per our construction of $\Phi_{\mathrm{u,cc}}$, we are concerned with only one uniformly distributed point in $\mathcal{X}_C(\mathbf{y},\kappa/\sqrt{\pi c_2},\Psi_b)$ lying in the region $\mathcal{B}_r(\mathbf{o})\cap\mathcal{X}_C(\mathbf{y},\kappa/\sqrt{\pi c_2},\Psi_b)$. Hence, we write (45) as $K_1^{\mathrm{CC}}(r,\kappa)\simeq$

$$\begin{aligned}&\mathbb{E}\left[\frac{|\mathcal{B}_r(\mathbf{o})\cap\mathcal{X}_C(\mathbf{y},\frac{\kappa}{\sqrt{\pi c_2}},\Psi_b)|}{|\mathcal{X}_C(\mathbf{y},\frac{\kappa}{\sqrt{\pi c_2}},\Psi_b)|}\right]=\mathbb{E}\left[\frac{S_C(r_m,r,\kappa)}{X_{C0}(1,\frac{\kappa}{\sqrt{\pi c_2}})}\right]\\ \approx&\mathbb{E}_{R_m}\left[S_C(r_m,r,\kappa)\right]\mathbb{E}\left[X_{C0}(1,\frac{\kappa}{\sqrt{\pi c_2}})^{-1}\right],\end{aligned}$$

where $S_C(r_m,r,\kappa)$ denotes the area of the region $\mathcal{B}_r(\mathbf{o})\cap\mathcal{B}_{R_c}(\mathbf{y})\cap((\mathbb{R}-r_m)^+\times\mathbb{R})$, and the last approximation follows from independence assumption between $S_C(r_m,r,\kappa)$ and $X_{C0}(1,\kappa/\sqrt{\pi c_2})^{-1}$. Now, using the result presented in Appendix C, we write

$$\begin{aligned}&\mathbb{E}_{R_m}\left[S_C(r_m,r,\kappa)\right]\\ \simeq&\mathbf{1}(R_c>r)\frac{\pi^2r^4}{2}+\mathbf{1}(R_c\le r)\pi^2R_c^2r^2-\frac{\pi^2R_c^4}{2},r\to 0,\end{aligned}\tag{46}$$

where $R_c=\kappa/\sqrt{\pi c_2}$. The first inverse moment of $X_{C0}(1,\kappa/\sqrt{\pi c_2})$ can be evaluated numerically using the approximated distribution presented in Sec. III. Now, the K-function is given as $K_1^{\mathrm{CC}}(r,\kappa)\simeq$

$$\begin{cases}\frac{\pi^2r^4}{2}\mathbb{E}\left[X_{C0}(1,\frac{\kappa}{\sqrt{\pi c_2}})^{-1}\right] & R_c>r,r\to 0\\ (\pi^2R_c^2r^2-\frac{\pi^2R_c^4}{2})\mathbb{E}\left[X_{C0}(1,\frac{\kappa}{\sqrt{\pi c_2}})^{-1}\right] & R_c\le r,r\to 0,\end{cases}$$

and the PCF is given as $g_1^{\mathrm{CC}}(r,\kappa)=$

$$\frac{\mathrm{d}K_1^{\mathrm{CC}}(r,\kappa)}{2\pi r\mathrm{d}r}\simeq\begin{cases}\pi r^2\mathbb{E}\left[X_{C0}(1,\frac{\kappa}{\sqrt{\pi c_2}})^{-1}\right] & R_c>r,r\to 0\\ \pi R_c^2\mathbb{E}\left[X_{C0}(1,\frac{\kappa}{\sqrt{\pi c_2}})^{-1}\right] & R_c\le r,r\to 0.\end{cases}$$

Note that as $R_c\to 0$, the 0-th BSs observes user locations that are almost identical to BS locations, which is a homogeneous PPP. In this case, when $R_c\to 0$, $\mathbb{E}\left[X_{C0}(1,\kappa/\sqrt{\pi c_2})^{-1}\right]\simeq\frac{1}{\pi R_c^2}$. Hence, $g_1^{\mathrm{CC}}(r,\kappa)\to 1$ as expected for a homogeneous PPP.

Using the asymptotic result that $1-\exp(-u)\simeq u$ as $u\to 0$, we write

$$\begin{aligned}g_1^{\mathrm{CC}}(r,\kappa)\simeq&\left(1-e^{-\pi r^2\mathbb{E}\left[X_{C0}\left(1,\frac{\kappa}{\sqrt{\pi c_2}}\right)^{-1}\right]}\right)\mathbf{1}(r<R_c)\\ &+\mathbf{1}(r\ge R_c),\end{aligned}$$

as $r\to 0$. Accordinng to the simulation based observation mentioned in [26], due to the condition $r\to 0$, the Voronoi cell $\mathcal{V}_{\Psi_b}(\mathbf{y})$ is skewed whose area is likely to be half of the area of a typical Voronoi cell. Similar argument can be made for the area of the CC region as well. Hence, a factor of 2 needs to be introduced for the first condition. Using this fact, for any value of r, a reasonable approximation for the PCF is $g_1^{\mathrm{CC}}(r,\kappa)\approx 1-\exp(-2\pi r^2\mathbb{E}\left[X_{C0}(1,\kappa/\sqrt{\pi c_2})^{-1}\right])$. ■

C. Proof of (46)

Depending on the value of R_c and r we have the following two cases of interest:

Case 1: $r<R_c$: The result for this case is obtained from [26, Lemma 2], and is given as

$$\mathbb{E}_{R_m}\left[S_C(r_m,r,\kappa)\right]\simeq\frac{\pi^2r^4}{2},\quad r\to 0.$$

Case 2: $r\ge R_c$: In this case, the area of the region $\mathcal{B}_r(\mathbf{o})\cap\mathcal{X}_C(\mathbf{y},\kappa/\sqrt{\pi c_2},\Psi_b)$ is given as $S_C(r_m,r,\kappa)=$

$$\begin{cases}r^2\left(u-\frac{\sin 2u}{2}\right)+R_c^2\left(v-\frac{\sin 2v}{2}\right)\\ \quad-(wR_c^2-r_m\sqrt{R_c^2-r_m^2}), & R_c\ge r_m\\ r^2u-\frac{r^2}{2}\sin 2u+R_c^2v-\frac{R_c^2}{2}\sin 2v, & R_c<r_m,\end{cases}$$

where $R_c=\kappa/\sqrt{\pi c_2}$, $u=\cos^{-1}\left(\frac{r^2+4r_m^2-R_c^2}{4rr_m}\right)$, $v=\cos^{-1}\left(\frac{R_c^2+4r_m^2-r^2}{4R_cr_m}\right)$, and $w=\cos^{-1}\left(\frac{r_m}{R_c}\right)$. Averaging over the random variable R_m, we get

$$\begin{aligned}\mathbb{E}\left[S_C(r_m,r,\kappa)\right]=&\pi R_c^2\int_0^{(r-R_c)/2}f_{R_m}(r_m)\mathrm{d}r_m\\ &+\int_{(r-R_c)/2}^{(r+Rc)/2}S_C(r_m,r,\kappa)f_{R_m}(r_m)\mathrm{d}r_m,\end{aligned}$$

where we have used the fact that for $r>2r_m+R_c$, $S_C(r_m,r,\kappa)=\pi R_c^2$. Further, note that for $2r_m>r+R_c$, $S_C(r_m,r,\kappa)=0$. Hence, the upper limit is introduced to consider the values of R_m for which $S_C(r_m,r,\kappa)\neq 0$. In addition, we use the asymptotic approximation $f_{R_m}(r_m)=8\pi r_m\exp(-4\pi r_m^2)\simeq 8\pi r_m(1-4\pi r_m^2)$, as $r_m\to 0$. After performing the integration, we obtain $\mathbb{E}\left[S_C(r_m,r,\kappa)\right]\simeq$

$$\begin{aligned}&\frac{\pi^2R_c^2r^4}{2}-\frac{\pi^2R_c^4r^2}{2}+\pi^2R_c^2r^2-\left(\frac{\pi^3R_c^2r^4}{2}+\frac{\pi^2R_c^4}{2}+\frac{\pi^3R_c^6}{2}\right)\\ \simeq&\pi^2R_c^2r^2-\frac{\pi^2R_c^4}{2},\quad r\to 0.\end{aligned}$$

This completes the proof of (46). ■

D. Derivation of Lemma 10

The proof can be done on the similar lines as that of Appendices B and C. In this case, the Ripley's K-function is given as

$$\begin{aligned}K_1^{\mathrm{CE}}(r,\kappa)\approx&\mathbb{E}_{R_m}\left[S_E(r_m,r,\kappa)|\mathcal{E}_3^C\right]\\ &\mathbb{E}\left[X_{E0}\left(1,\frac{\kappa}{\sqrt{\pi c_2}}\right)^{-1}\middle|\mathcal{E}_3^C\right],\quad r\to 0,r>R_c.\end{aligned}$$

Asymptotically, conditioned on $\mathcal{E}_3^C$, the distribution of R_m is given as

$$F_{R_m}(r_m|R_M > R_c) = \frac{\mathbb{P}\left[R_m \leq r_m, R_M > R_c\right]}{\mathbb{P}\left[R_M > R_c\right]} \simeq \mathbb{P}\left[R_m \leq r_m\right], \quad R_c \to 0.$$

The condition $R_c \to 0$ is of interest to us as our goal is to find the PCF for $r \to 0$, and $r > R_c$. Now, the following expectation

$$\begin{aligned}
&\mathbb{E}_{R_m}\left[S_E(r_m, r, R_c)|\mathcal{E}_3^C\right] \\
\simeq &\int_0^r A_1(r, r_m, R_c)\mathrm{d}F_{R_m}(r_m) - \int_0^{(r-R_c)/2} A_2(r, r_m, R_c)\mathrm{d}F_{R_m}(r_m) \\
&- \int_{(r-R_c)/2}^{(r+R_c)/2} A_2(r, r_m, R_c)\mathrm{d}F_{R_m}(r_m) - \int_0^{R_c} A_3(r, r_m, R_c)\mathrm{d}F_{R_m}(r_m) \\
= &\frac{\pi^2 r^4}{2} + \frac{\pi^3 r^6}{2} - \frac{\pi^2 R_c^2 r^4}{2} + \frac{\pi^2 R_c^4 r^2}{2} \\
&- \pi^2 R_c^2 r^2 + \frac{\pi^3 R_c^2 r^4}{2} + \frac{\pi^2 R_c^4}{2} + \frac{\pi^3 R_c^6}{2} \\
\simeq &\frac{\pi^2(r^4 + R^4 - 2R_c^2 r^2)}{2},
\end{aligned}$$

where the last step follows from neglecting the 6-th order terms. In the previous expression

$$\begin{aligned}
A_1(r, r_m, R_c) =& r^2 \arccos\frac{r_m}{r} - r_m\sqrt{r^2 - r_m^2}, \\
A_2(r, r_m, R_c) =& \left(r^2 u - \frac{r^2\sin(2u)}{2} + R_c^2 v - \frac{R_c^2\sin(2v)}{2}\right) \\
&\mathbf{1}\big(|2r_m - r| \leq R_c\big) + \pi R_c^2 \mathbf{1}\big(r_m < \frac{r - R_c}{2}\big), \\
A_3(r, r_m, R_c) =& \left(R_c^2 \arccos\left(\frac{r_m}{R_c}\right) - r_m\sqrt{R_c^2 - r_m^2}\right)\times \\
&\mathbf{1}\left(r_m \leq R_c\right).
\end{aligned}$$

Using the above result, the Ripley's K-function is given as $K_1^{\mathrm{CE}}(r, \kappa) \simeq$

$$\frac{\pi^2\left(r^2 - R_c^2\right)^2}{2}\mathbb{E}\left[X_{E0}(1, \frac{\kappa}{\sqrt{\pi c_2}})^{-1}\middle|\mathcal{E}_3^C\right], \; r > R_c, r \to 0. \tag{47}$$

Hence, the PCF is given as

$$\begin{aligned}
g_1^{\mathrm{CE}}(r, \kappa) =& \frac{\mathrm{d}K_1^{\mathrm{CE}}(r, \kappa)}{2\pi r \; \mathrm{d}r} \\
\simeq& \pi\left(r^2 - R_c^2\right)\mathbb{E}\left[X_{E0}\left(1, \frac{\kappa}{\sqrt{\pi c_2}}\right)\right)^{-1}\middle|\mathcal{E}_3^C\Bigg] \\
\approx& \frac{14\pi\left(r^2 - R_c^2\right)\mathbb{P}\left[\mathcal{E}_3^C\right]}{5\exp(-\pi R_c^2)},
\end{aligned}$$

where the intuition for the approximation in the last step follows from Jensen's inequality

$$\mathbb{E}\left[X_{E0}\left(1, \frac{\kappa}{\sqrt{\pi c_2}}\right)^{-1}\middle|\mathcal{E}_3^C\right] \geq \frac{1}{\mathbb{E}\left[X_{E0}\left(1, \frac{\kappa}{\sqrt{\pi c_2}}\right)\middle|\mathcal{E}_3^C\right]}$$

$$= \exp(\pi R_c^2)\mathbb{P}\left[\mathcal{E}_3^C\right].$$

From [26], when $R_c = 0, \mathbb{E}\left[X_{E0}(1, \frac{\kappa}{\sqrt{\pi c_2}})^{-1}\right] \approx 14/5$. Hence, for $R_c \to 0$, we approximate

$$\begin{aligned}
\mathbb{E}\left[X_{E0}(1, \frac{\kappa}{\sqrt{\pi c_2}})^{-1}|\mathcal{E}_3^C\right] \approx& 14/5\exp(\pi R_c^2)\mathbb{P}\left[\mathcal{E}_3^C\right] \\
=& 14/5\exp(\kappa^2/c_2)\mathbb{P}\left[\mathcal{E}_3^C\right].
\end{aligned}$$

This completes the proof of the Lemma. ■

REFERENCES

[1] P. Parida and H. S. Dhillon, "Johnson-Mehl cell-based analysis of UL cellular network with coupled user and BS locations," in *Proc., IEEE Intl. Conf. on Commun. (ICC)*, Kansas City, USA, May 2018.

[2] T. L. Marzetta, "Noncooperative cellular wireless with unlimited numbers of base station antennas," *IEEE Trans. on Wireless Commun.*, vol. 9, no. 11, pp. 3590–3600, Nov. 2010.

[3] E. Bjornson, E. G. Larsson, and T. L. Marzetta, "Massive MIMO: ten myths and one critical question," *IEEE Commun. Magazine*, vol. 54, no. 2, pp. 114–123, February 2016.

[4] E. Bjornson, J. Hoydis, and L. Sanguinetti, "Massive MIMO has unlimited capacity," *IEEE Trans. on Wireless Commun.*, vol. 17, no. 1, pp. 574–590, Jan 2018.

[5] F. Fernandes, A. Ashikhmin, and T. L. Marzetta, "Inter-cell interference in noncooperative TDD large scale antenna systems," *IEEE Journal on Sel. Areas in Commun.*, vol. 31, no. 2, pp. 192–201, February 2013.

[6] H. Yin, D. Gesbert, M. Filippou, and Y. Liu, "A coordinated approach to channel estimation in large-scale multiple-antenna systems," *IEEE Journal on Sel. Areas in Commun.*, vol. 31, no. 2, pp. 264–273, February 2013.

[7] J. Jose, A. Ashikhmin, T. L. Marzetta, and S. Vishwanath, "Pilot contamination and precoding in multi-cell TDD systems," *IEEE Trans. on Wireless Commun.*, vol. 10, no. 8, pp. 2640–2651, August 2011.

[8] J. H. Sorensen and E. de Carvalho, "Pilot decontamination through pilot sequence hopping in massive MIMO systems," in *Proc., IEEE Globecom*, Dec 2014, pp. 3285–3290.

[9] A. S. Alwakeel and A. H. Mehana, "Achievable rates in uplink massive MIMO systems with pilot hopping," *IEEE Trans. on Commun.*, vol. PP, no. 99, pp. 1–1, 2017.

[10] O. Elijah, C. Y. Leow, T. A. Rahman, S. Nunoo, and S. Z. Iliya, "A comprehensive survey of pilot contamination in massive MIMO - 5G system," *IEEE Commun. Surveys and Tutorials*, vol. 18, no. 2, pp. 905–923, Secondquarter 2016.

[11] Y. Li, Y.-H. Nam, B. L. Ng, and J. Zhang, "A non-asymptotic throughput for massive MIMO cellular uplink with pilot reuse," in *Proc., IEEE Globecom*, Dec 2012, pp. 4500–4504.

[12] E. Bjornson, E. G. Larsson, and M. Debbah, "Massive MIMO for maximal spectral efficiency: How many users and pilots should be allocated?" *IEEE Trans. on Wireless Commun.*, vol. 15, no. 2, pp. 1293–1308, Feb 2016.

[13] I. Atzeni, J. Arnau, and M. Debbah, "Fractional pilot reuse in massive MIMO systems," in *Proc., IEEE Intl. Conf. on Commun. Workshops (ICC Workshops)*, June 2015, pp. 1030–1035.

[14] J. G. Andrews, A. K. Gupta, and H. S. Dhillon, "A primer on cellular network analysis using stochastic geometry," 2016. [Online]. Available: http://arxiv.org/abs/1604.03183

[15] H. ElSawy, A. Sultan-Salem, M. S. Alouini, and M. Z. Win, "Modeling and analysis of cellular networks using stochastic geometry: A tutorial," *IEEE Commun. Surveys and Tutorials*, vol. 19, no. 1, pp. 167–203, Firstquarter 2017.

[16] P. Madhusudhanan, X. Li, Y. Liu, and T. X. Brown, "Stochastic geometric modeling and interference analysis for massive MIMO systems," in *Proc., Modeling and Optimization in Mobile, Ad Hoc and Wireless Networks*, May 2013, pp. 15–22.

[17] S. Govindasamy, "Uplink performance of large optimum-combining antenna arrays in Poisson-cell networks," in *Proc., IEEE Intl. Conf. on Commun. (ICC)*, Jun. 2014, pp. 2158–2164.

[18] T. Bai and R. W. Heath, "Asymptotic coverage and rate in massive MIMO networks," in *IEEE Global Conf. on Signal and Inform. Processing*, Dec 2014, pp. 602–606.

[19] ——, "Asymptotic SINR for millimeter wave massive MIMO cellular networks," in *Proc., IEEE SPAWC*, June 2015, pp. 620–624.

[20] S. Govindasamy, "Uplink performance of large optimum-combining antenna arrays in power-controlled cellular networks," in *Proc., IEEE Intl. Conf. on Commun. (ICC)*, Jun. 2015, pp. 4137–4143.

[21] T. Bai and R. W. Heath, "Analyzing uplink SINR and rate in massive MIMO systems using stochastic geometry," *IEEE Trans. on Commun.*, vol. 64, no. 11, pp. 4592–4606, Nov 2016.

[22] E. Bjornson, L. Sanguinetti, and M. Kountouris, "Deploying dense networks for maximal energy efficiency: Small cells meet massive MIMO," *IEEE Journal on Sel. Areas in Commun.*, vol. 34, no. 4, pp. 832–847, Apr 2016.

[23] N. Liang, W. Zhang, and C. Shen, "An uplink interference analysis for massive mimo systems with MRC and ZF receivers," in *Proc., IEEE Wireless Commun. and Networking Conf. (WCNC)*, Mar. 2015, pp. 310–315.

[24] A. Shojaeifard, K. Wong, M. D. Renzo, G. Zheng, K. A. Hamdi, and J. Tang, "Massive MIMO-enabled full-duplex cellular networks," *IEEE Trans. on Commun.*, vol. 65, no. 11, pp. 4734–4750, Nov 2017.

[25] O. Y. Bursalioglu, G. Caire, R. K. Mungara, H. C. Papadopoulos, and C. Wang, "Fog massive MIMO: A user-centric seamless hot-spot architecture," 2018. [Online]. Available: http://arxiv.org/abs/1803.07614

[26] M. Haenggi, "User point processes in cellular networks," *IEEE Wireless Commun. Letters*, vol. 6, no. 2, pp. 258–261, April 2017.

[27] ——, *Stochastic Geometry for Wireless Networks*. Cambridge University Press, 2013.

[28] J. Moller, "Random Johnson-Mehl Tessellations," *Advances in Applied Probability*, vol. 24, no. 4, pp. 814–844, 1992.

[29] B. Yu, S. Mukherjee, H. Ishii, and L. Yang, "Dynamic TDD support in the LTE-B enhanced local area architecture," in *Proc., IEEE Globecom Workshops*, Dec 2012, pp. 585–591.

[30] H. Q. Ngo, E. Larsson, and T. Marzetta, "Energy and spectral efficiency of very large multiuser MIMO systems," *IEEE Trans. on Commun.*, vol. 61, no. 4, pp. 1436–1449, Apr. 2013.

[31] E. Pineda and D. Crespo, "Temporal evolution of the domain structure in a Poisson-Voronoi transformation," *Journal of Statistical Mechanics: Theory and Experiment*, vol. 2007, no. 06, p. P06007, 2007.

[32] S. M. Yu and S. Kim, "Downlink capacity and base station density in cellular networks," in *11th International Symposium and Workshops on Modeling and Optimization in Mobile, Ad Hoc and Wireless Networks (WiOpt)*, May 2013, pp. 119–124.

[33] S. Singh, H. S. Dhillon, and J. G. Andrews, "Offloading in heterogeneous networks: Modeling, analysis, and design insights," *IEEE Trans. on Wireless Commun.*, vol. 12, no. 5, pp. 2484–2497, May 2013.

[34] P. Calka, "The distributions of the smallest disks containing the Poisson-Voronoi typical cell and the Crofton cell in the plane," *Advances in Applied Probability*, vol. 34, no. 4, pp. 702–717, 2002.

[35] J. Gil-Pelaez, "Note on the inversion theorem," *Biometrika*, vol. 38, no. 3-4, pp. 481–482, 1951.

[36] M. D. Renzo and P. Guan, "Stochastic geometry modeling of coverage and rate of cellular networks using the Gil-Pelaez inversion theorem," *IEEE Commun. Lett.*, vol. 18, no. 9, pp. 1575–1578, Sep. 2014.

[37] J. Schloemann, H. S. Dhillon, and R. M. Buehrer, "Toward a tractable analysis of localization fundamentals in cellular networks," *IEEE Trans. on Wireless Commun.*, vol. 15, no. 3, pp. 1768–1782, Mar. 2016.

[38] K. A. Hamdi, "A useful lemma for capacity analysis of fading interference channels," *IEEE Trans. on Commun.*, vol. 58, no. 2, 2010.

[39] M. D. Renzo, A. Guidotti, and G. E. Corazza, "Average rate of downlink heterogeneous cellular networks over generalized fading channels: A stochastic geometry approach," *IEEE Trans. on Commun.*, vol. 61, no. 7, pp. 3050–3071, July 2013.

[40] Z. Yazdanshenasan, H. S. Dhillon, M. Afshang, and P. H. J. Chong, "Poisson hole process: Theory and applications to wireless networks," *IEEE Trans. on Wireless Commun.*, vol. 15, no. 11, pp. 7531–7546, Nov 2016.

Priyabrata Parida Priyabrata Parida (S'14) received the B. Tech degree in Electronics and Communications Engineering from the National Institute of Technology, Durgapur, India, in 2010 and the M.S. degree in Telecommunications from Indian Institute of Technology, Kharagpur, India, in 2015. He is currently a Ph.D. student at Virginia Tech, where his research interest includes modeling and analysis of fifth generation cellular networks using tools from stochastic geometry. His other research interest includes MIMO and resource allocation in wireless systems. He has held internship positions at MediaTek Inc., San Jose, USA and Blue Danube Systems Inc., Santa Clara, USA during summer 2016 and 2018, respectively. He was awarded Exemplary Reviewer of IEEE TRANSACTIONS ON WIRELESS COMMUNICATIONS in 2017.

Harpreet S. Dhillon (S'11–M'13) received the B.Tech. degree in Electronics and Communication Engineering from IIT Guwahati, India, in 2008; the M.S. degree in Electrical Engineering from Virginia Tech, Blacksburg, VA, USA, in 2010; and the Ph.D. degree in Electrical Engineering from the University of Texas at Austin, TX, USA, in 2013. In academic year 2013-14, he was a Viterbi Postdoctoral Fellow at the University of Southern California, Los Angeles, CA, USA. He joined Virginia Tech in August 2014, where he is currently an Assistant Professor and Steven O. Lane Junior Faculty Fellow of Electrical and Computer Engineering. He has held short-term visiting positions at Bell Labs, Samsung Research America, Qualcomm Inc., and Politecnico di Torino. His research interests include communication theory, stochastic geometry, geolocation, and wireless *ad hoc* and heterogeneous cellular networks.

Dr. Dhillon is a Clarivate Analytics Highly Cited Researcher and has coauthored five best paper award recipients including the 2016 IEEE Communications Society (ComSoc) Heinrich Hertz Award, the 2015 IEEE ComSoc Young Author Best Paper Award, the 2014 IEEE ComSoc Leonard G. Abraham Prize, and two conference best paper awards at IEEE ICC 2013 and European Wireless 2014. He was named the 2018 College of Engineering Faculty Fellow and the 2017 Outstanding New Assistant Professor by Virginia Tech. His other academic honors include the 2013 UT Austin Wireless Networking and Communications Group (WNCG) leadership award, the UT Austin Microelectronics and Computer Development (MCD) Fellowship, and the 2008 Agilent Engineering and Technology Award. He currently serves as an Editor for the IEEE TRANSACTIONS ON WIRELESS COMMUNICATIONS, the IEEE TRANSACTIONS ON GREEN COMMUNICATIONS AND NETWORKING, and the IEEE WIRELESS COMMUNICATIONS LETTERS.